Quantum mechanical-like approach with non-Hermitian effective Hamiltonians in spin-orbit coupled optical cavities

Przemysław Oliwa [1], Witold Bardyszewski [2,*] and Jacek Szczytko [1,†]

[1]*Institute of Experimental Physics, Faculty of Physics, University of Warsaw, Ul. Pasteura 5, 02-093 Warsaw, Poland*
[2]*Institute of Theoretical Physics, Faculty of Physics, University of Warsaw, Ul. Pasteura 5, 02-093 Warsaw, Poland*

We present a comprehensive analytical model of resonant states in birefringent microcavities with permeable mirrors. We derive an effective, non-Hermitian photonic Hamiltonian describing cavity mode dispersion and modal lifetimes by applying the Green's function technique based on the Mittag-Leffler expansion with respect to the resonant states and the $\boldsymbol{k} \cdot \boldsymbol{p}$ perturbation theory known from semiconductor physics. Using this formalism we obtained results which can be interpreted as effective cavity mode spin-orbit coupling. We use this method to derive the two-mode Hamiltonian to describe the properties of light in the cavity, which significantly reduces the computational effort and properly captures the polarization of the eigenmodes. This is done by introducing the necessary corrections to the Hamiltonian matrix and modifying the basis modes resulting from the coupling with other optical modes present in the system. This simplified Hamiltonian allows us to determine the positions of exceptional points in momentum space. These points are connected by Fermi arcs and appear due to non-Hermiticity and $\mathcal{PT}$ symmetry.

I. INTRODUCTION

Although the propagation of electromagnetic waves in optical devices can be successfully described using Maxwell's equations, there is a growing tendency to reformulate this problem into a framework resembling quantum mechanics by introducing the wave function of photons [1], the Weyl eigenvalue equation for electric and magnetic fields [2,3], and the spin-orbit interaction (SOI) of light [3–6]. This quantum mechanical-like approach has been especially useful in the description of periodic photonic structures and light polarization and propagation in low-dimensional systems such as open optical systems [7,8], two-dimensional optical cavities, waveguides, and fibers [9] and in topological photonics [10,11]. For example, the properties of a polarized electromagnetic wave propagating in one- or two-dimensional structures can be successfully described using the effective two-mode Hamiltonian corresponding to a massive particle with spin 1/2 represented by Pauli matrices [12]. Such an approach simplifies theoretical description but also allows for enormous progress in modern photonics by exploiting the correspondence between the mathematical similarity of equations of propagating electromagnetic waves and electrons in condensed matter. For instance, the optical spin Hall effect

has been predicted in optical microcavities [13] and observed experimentally [14,15], and the effective Hamiltonian of the Rashba-Dresselhaus (RD) optical analog of SOI has been demonstrated [16], leading to RD optical activity [17–21], RD magnetic field [22] and RD lasing [23] and coupling of light and matter [24–26]. Effective Hamiltonians are widely used to express exceptional and Dirac points in the dispersion relation of photons [27–29], Berry phases [30,31], quantum geometric tensor [32] and polarization textures [33]. Finally, non-Hermitian physics [34–36] has been analyzed in terms of imaginary elements added in a Hamiltonian. Although the effective Hamiltonians have proven their usefulness, their form was guessed (for instance, using arguments about the symmetry of the investigated system) rather than rigorously derived. In this paper, we present a comprehensive method for analyzing polarization of light in widely used physical systems such as optical resonators and other open optical systems. In order to study the SOI of light, we consider the anisotropic (birefringent) medium filling the inside of a planar cavity. We apply the Green's function method based on Mittag-Leffler expansion with respect to resonant states [37]. With this method, we propose an effective way to describe the modal dispersion and the modal electric field, which can be related to experimental studies of light polarization in such systems. An element of our two-level model is the inclusion of coupling with other modes, which significantly modifies the profile of the electric field in the cavity. It turns out that taking these modifications into account is necessary for the correct description of the polarization properties of light in the cavity, and thus also for the correct determination of the quantum geometric tensor. We compare the proposed method with a numerical Berreman-Schubert transfer matrix calculation of light propagation through cavities [38,39].

---

*witold.bardyszewski@fuw.edu.pl
†jacek.szczytko@fuw.edu.pl

The modern optical cavities which are widely used in the study of the optical properties of exciton polariton condensates can be considered as systems of parallel plates [40,41]. The propagation of light through such an optical system is fully determined by the appropriate optical dielectric tensors of each plate and the proper matching conditions imposed upon the electromagnetic field at the interfaces between them. In the simplest case of a monochromatic, fully polarized light wave, which is incident perpendicularly on the plate, we can be concerned only with its electric field component. In this case, it follows from Maxwell's equations that the electric field and its derivative along the propagation direction should be continuous across the interface. The state of polarization is fully determined by the electric field and therefore it is convenient to characterize the propagating wave in terms of the two-dimensional Jones vectors. The effect of propagation through a system of parallel plates is then represented as a linear operator acting on the vectors. This particular optical system bears an obvious analogy with quantum mechanics in one dimension, as was already pointed out in the original paper by Jones [42].

The simple description using the Jones vectors may become impractical for the obliquely incident light since in this case the boundary conditions for the electric and the magnetic fields cannot be easily separated. In this situation one can consider two electric and two magnetic field components which are parallel to the plate. At the cost of doubling the dimension of the problem, one obtains a system of first-order differential equations with respect to the propagation direction variable z with elementary continuity condition of the four components at each interface. This method, proposed by Berreman [38] and modified by Schubert [39], is numerically exact and allows for solving the transmission and reflection problem for any value of the angle of incidence.

The numerical modeling of transmission and reflection of multilayered media is accomplished using the transfer matrix method, where each successive layer included in the structure is represented by a transfer matrix. In such a way the description of propagation of the electromagnetic wave by microcavity is based on the multiplication of several dozen matrices in order to get the reflection and transmission coefficient for one certain angle of the incident wave and one certain energy of this wave. To obtain typical reflectance spectra for the cavity one has to perform calculations for a range of angles and energies of the incident light, so a very long computation time is needed. However, the results obtained during the simulation almost perfectly reflect the experimental results [15,16,33,43].

Obviously, despite its accuracy, this method in most situations brings a lot of redundant information which has to be eventually filtered out and the numerical results are not always easily interpreted. When the angle of incidence is narrow, which is the case for most experiments involving optical cavities, the fully blown Berreman method based on the operation on 4×4 matrices looks like overkill. In this paper we propose to go back to the Jones description of the electromagnetic wave for small incidence angles, due to its simple connection to the polarization of light. We propose to use a perturbation scheme in which the reference "unperturbed" case corresponds to the propagation through a properly chosen

isotropic medium while the modifications due to the birefringence are treated as a perturbation. For this purpose, we have replaced the system of first-order differential Maxwell's equations with an equivalent set of second-order equations for the electric field alone. At this stage, no information relative to the original equations was lost. In particular, matching conditions for the derivative of the electric field reflect the continuity of the magnetic field. Since we intended to narrow our model to the range of small incidence angles, we have applied an expansion up to second order with respect to the ratio of parallel and perpendicular wave vectors and therefore all the effects related to the propagation of light through the cavity are determined within this accuracy.

In the case of the optical microcavity we are interested mostly in the resonant states, i.e., in the states corresponding to the maximum of transmission. We will be looking for energy dispersion $\mathrm{Re}(E_s(\boldsymbol{k}))$ and inverse lifetimes $-\mathrm{Im}(E_s(\boldsymbol{k}))$ of those states as functions of propagation angles and polarization. A good example is the resonant modes in an ideal Fabry-Pérot resonator filled with a birefringent medium in the form of a nematic liquid crystal [16,33]. In this case, the dispersion relations $E_s(\boldsymbol{k})$ for linear polarizations $s = X, Y$ defined for small in-plane wave vectors $\boldsymbol{k}_\parallel = (k_x, k_y)$, neglecting the k-dependent coupling between modes, are approximately paraboloidal in shape [Fig. 1(a)]:

$$E_s(\boldsymbol{k}) = \frac{\hbar c}{n_s} |\boldsymbol{k}| = \frac{\hbar c}{n_s} \sqrt{k_z^2 + \boldsymbol{k}_\parallel^2} \approx E_{sm} + \frac{\hbar^2 \boldsymbol{k}_\parallel^2}{2 m_s^*}, \quad (1)$$

where n_s is the polarization-dependent refractive index inside the ideal Fabry-Pérot resonator; $k_z = m\pi/L$, where m is the mode number and L is the cavity thickness; $E_{sm} = \hbar c m \pi/(n_s L)$ and $m_s^* = \hbar N \pi n_s/(cL)$; and c is the speed of light [40,41]. One can already notice that the dispersion relation in Eq. (1) has a form resembling the energy-momentum dispersion relation of a massive particle in typical solid-state problems, where the polarization-dependent *effective mass* m_s^* is an analog of the effective mass of an electron in a semiconductor. Analyzing the coupling between two modes close in energy at $\boldsymbol{k}_\parallel = 0$ (perpendicular incidence), we have proposed an analytical expression for energy dispersion as a function of wave vector (angle of incident light) by diagonalizing appropriate "effective Hamiltonians" [16]. Using this approach derived for a perfect optical cavity we have been able to interpret phenomena such as optical merons [33] and the optical persistent spin helix [23,43].

Now we extend our previous approach to the case of microcavities with realistic mirrors admitting resonant states with finite lifetimes. We present and discuss in detail our model, which combines the features of the analytical two-mode approach and the full numerical model used in Schubert's considerations. The necessary steps towards our derivation are represented schematically in Fig. 1. We describe resonant states in birefringent cavities in terms of the retarded Green's function. We will start with the simplest version of the Hamiltonian already mentioned [Fig. 1(a)] [16], which describes two linearly polarized modes with infinite lifetimes in an ideal Fabry-Pérot resonator. The polarization state of the modal electric field $\boldsymbol{E}$ (the eigenmode in the cavity) can be fully characterized by the set of Stokes parameters (S_0, S_1, S_2, S_3),
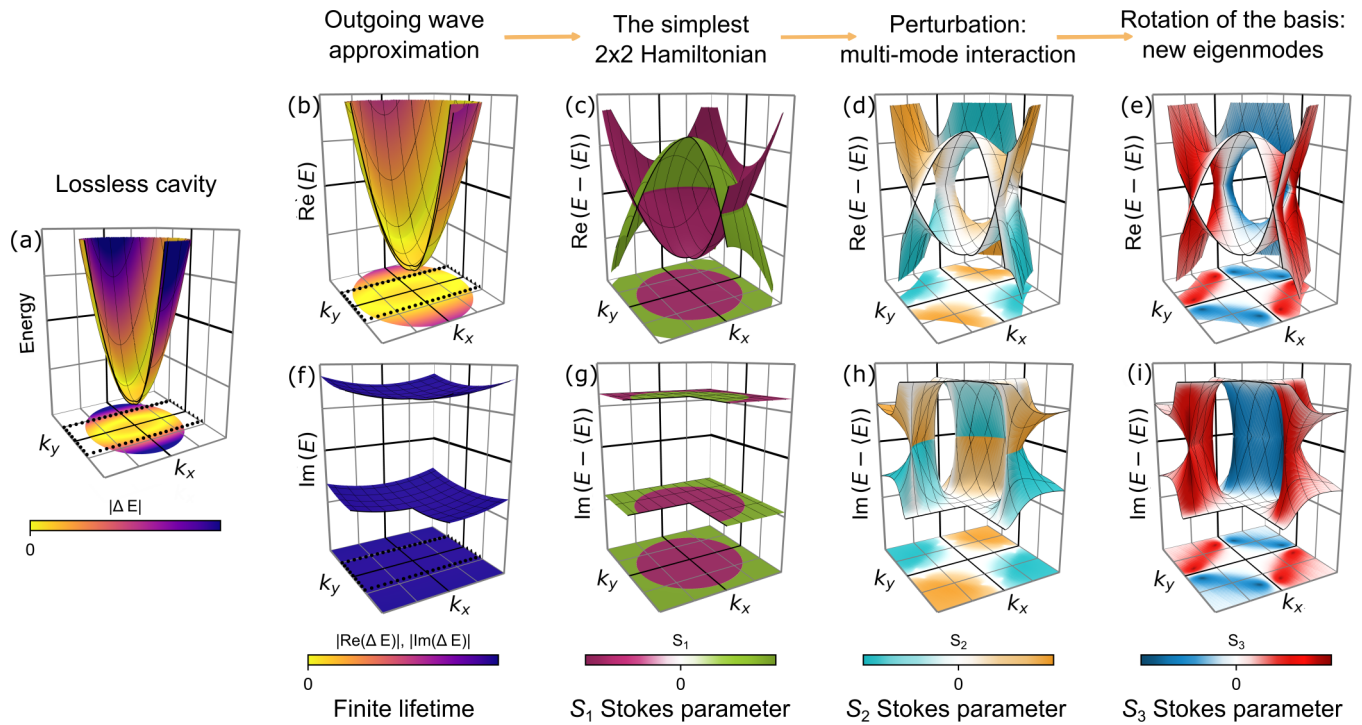
FIG. 1. The scheme of the analysis of the dispersion relation $E(\mathbf{k})$ of two optical modes in a Fabry-Pérot resonator: (a) the results obtained using the simplest 2×2 Hamiltonian matrix corresponding to two linearly polarized modes with infinite lifetime in an ideal Fabry-Pérot resonator neglecting the k-dependent coupling between modes, Eq. (1). [(b) and (f)] the energy $\mathrm{Re}(E)$ and broadening $\mathrm{Im}(E)$ of resonant modes obtained using this Hamiltonian and the outgoing wave boundary conditions in a cavity with permeable mirrors. The modes are linearly polarized as depicted by the s_1 Stokes parameter in color scale in (c) and (g). [(d) and (h)] Results obtained with the effective Hamiltonian matrix modified by inclusion of coupling with other modes leading to rotation of the linear polarization plane (nonzero s_2 Stokes parameter); [(e) and (i)] Correcting of the basis modes by inclusion of coupling with other modes leads to further rotation of the modal fields resulting in nonzero s_3 Stokes parameter, corresponding to the circular component of polarization. The quarter of the dispersion relation was removed to allow access to the center of $\mathbf{k}$ space. In images (c)–(e) and (g)–(i) the arithmetic mean of modal energies, $\langle E \rangle$, was subtracted to show four double exceptional points.

where $S_0 = \mathbf{E}^\dagger \boldsymbol{\sigma}_0 \mathbf{E}$ is the total intensity of light with $\boldsymbol{\sigma}_0$ denoting the 2×2 unit matrix and $S_i = \mathbf{E}^\dagger \boldsymbol{\sigma}_i \mathbf{E}$ with Pauli matrices $\boldsymbol{\sigma}_1 = \boldsymbol{\sigma}_z$, $\boldsymbol{\sigma}_2 = \boldsymbol{\sigma}_x$, and $\boldsymbol{\sigma}_3 = \boldsymbol{\sigma}_y$. In the standard approach, Stokes polarization parameters are normalized as ($i \geqslant 1$)

$$s_i = \frac{S_i}{S_0}. \qquad (2)$$

Here s_1 is the degree of linear polarization in the horizontal-vertical direction (in this paper it corresponds to x, y coordinates), s_2 is the degree of linear polarization in the diagonal and antidiagonal direction, and s_3 is the degree of circular polarization. Next we consider a simple model of decoupled modes of the electromagnetic field in a cavity with permeable mirrors using outgoing wave boundary conditions resulting in the broadening of the photon dispersion [Figs. 1(b) and 1(f)]. The eigenstates are fully linearly polarized, as depicted by the s_1 Stokes parameter in color scale in Figs. 1(c) and 1(g). Next we introduce the corrections due to the k-dependent coupling between photonic modes as a perturbation. According to the perturbation theory for almost degenerate states, both the Hamiltonian matrix and the basis vectors are modified. The modification of the Hamiltonian matrix alone modifies the spectra and effectively rotates the polarization of the eigenstates, adding a nonzero s_2 component to the Stokes vector [Figs. 1(d) and 1(h)]. Finally, correction of

the basis modes, described in detail in Appendix E, adds a nonzero s_3 Stokes parameter related to the circular polarization [Figs. 1(e) and 1(i)].

Using our model we are able to demonstrate in particular how the complicated structure of Bragg mirrors (Fig. 2), which are the main element increasing computational time in the Schubert method, can be modeled with a delta func-
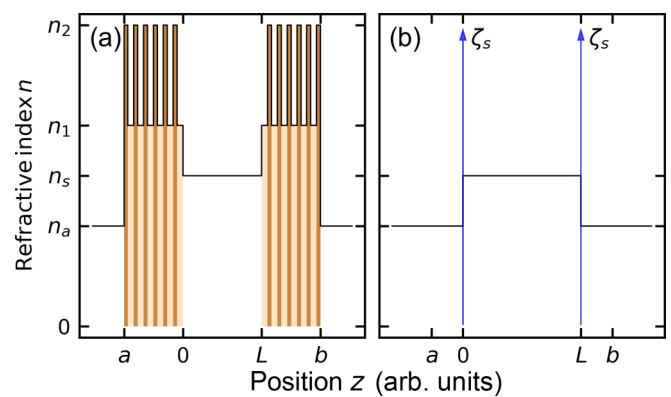

FIG. 2. Comparison of the refractive index profile in standard optical microcavity with (a) distributed Bragg reflectors and (b) the simplified version.

tion like refractive index profile, i.e., infinitely thin layers ($l \rightarrow 0$) with an infinite permittivity $\varepsilon_l \rightarrow \pm\infty$ and $l\varepsilon_l =$ const (Fig. 2). Such a simplified model of microcavity mirrors allows to obtain analytical solutions for characteristic quantities, such as the reflection or transmission coefficient and the electric field inside the cavity. As examples we will discuss three main cases of the interaction between almost degenerate modes of the same or different parities. It should be emphasized, however, that our method can be applied to any type of high-quality cavity mirror.

II. RESONANT STATES IN BIREFRINGENT CAVITIES

We consider the microcavity of width L filled with birefringent material (liquid crystal) enclosed between two Bragg mirrors shown in Fig. 2. The cavity layer is perpendicular to the z axis and extends from $z = 0$ to $z = L$. The mirrors are limited to the regions $a < z < 0$ and $L < z < b$. The coordinate system is chosen in which the x axis is directed horizontally and the y axis vertically in the cavity plane. The region outside the cavity is filled with the ambient refractive index $n_a = \sqrt{\varepsilon_a}$.

An optical cavity with permeable mirrors

Due to the translational symmetry of our system in the direction perpendicular to the z axis we can assume the projection of the electric field on the cavity plane in the form of a two-dimensional vector:

$$\begin{pmatrix} E_x(x, y, z) \\ E_y(x, y, z) \end{pmatrix} = \boldsymbol{E_k}(z)e^{i(\boldsymbol{k}\cdot\boldsymbol{r} - ck_0 t)}, \tag{3}$$

where $\boldsymbol{k}$ and $\boldsymbol{r}$ represent a two-dimensional wave vector and position vector, respectively, in the direction perpendicular to the z axis. The frequency of light is given by $\omega = ck_0$. By eliminating the magnetic field from the Maxwell equations we obtain the second-order equation for the electric field (Appendix D). Up to the term of the order k^2/k_0^2, the vector $\boldsymbol{E_k}$ in the general birefringent layer characterized by a real dielectric tensor ε_{ij} can by found from the following effective wave equation written in terms of the second-order differential operator $\hat{\boldsymbol{\mathcal{L}}}(z; \omega, \boldsymbol{k})$:

$$\hat{\boldsymbol{\mathcal{L}}}E = \left((\partial_z - \mathbf{A}^T)(\partial_z - \mathbf{A}) - \mathbf{B} + k_0^2\mathbf{B}_0\right)E = \mathbf{0}. \tag{4}$$

Assuming for simplicity that our coordinate system is oriented in such a way that $\varepsilon_{xy} = \varepsilon_{yx} = \varepsilon_{zy} = \varepsilon_{yz} = 0$, and introducing an effective refractive index squared for x polarization, $n_x^2 = \tilde{\varepsilon}_{xx} = \varepsilon_{xx} - \varepsilon_{xz}\varepsilon_{zx}/\varepsilon_{zz}$, we have

$$\mathbf{A} = \frac{-i\varepsilon_{xz}}{\varepsilon_{zz}} \begin{bmatrix} k_x & 0 \\ k_y & 0 \end{bmatrix}, \quad \mathbf{B}_0 = \mathbf{B}_0^T = \begin{bmatrix} \tilde{\varepsilon}_{xx} & 0 \\ 0 & \varepsilon_{yy} \end{bmatrix}, \tag{5a}$$

and

$$\mathbf{B} = \frac{1}{\varepsilon_{zz}} \begin{bmatrix} \tilde{\varepsilon}_{xx}k_x^2 + \varepsilon_{zz}k_y^2 & (\varepsilon_{yy} - \varepsilon_{zz})k_x k_y \\ (\tilde{\varepsilon}_{xx} - \varepsilon_{zz})k_x k_y & \varepsilon_{zz}k_x^2 + \varepsilon_{yy}k_y^2 \end{bmatrix}. \tag{5b}$$

The superscript T denotes a matrix transpose. The components of the dielectric tensor ε_{ij} in general depend on z. In the isotropic medium (e.g., in the ambient environment outside the cavity) the equations for the horizontal component E_x and vertical component E_y of the electric field are decoupled. We

note at this point that in our approximation, the z derivative of the electric field suffers a discontinuity at the interfaces with the birefringent medium. This discontinuity is linear in $\boldsymbol{k}$ as suggested by the presence of the matrix $\mathbf{A}$ in Eq. (4). The second-order contribution to this discontinuity is negligibly small.

The optical properties of the cavity for fixed light frequency ω and in-plane wave vector $\boldsymbol{k}$ are described in terms of the retarded Green's function for the operator $\hat{\boldsymbol{\mathcal{L}}}$:

$$\hat{\boldsymbol{\mathcal{L}}}(z; \omega, \boldsymbol{k})\mathbf{G}(z, z'; \omega, \boldsymbol{k}) = \delta(z - z')\boldsymbol{\sigma}_0, \tag{6}$$

with outgoing wave boundary conditions

$$\partial_z \mathbf{G}(z, z') = \begin{cases} -ik_z\mathbf{G}(z, z') & \text{for } z < \min(a, z') \\ ik_z\mathbf{G}(z, z') & \text{for } z > \max(b, z'), \end{cases} \tag{7}$$

where $k_z = \sqrt{\varepsilon_a k_0^2 - k^2}$.

The retarded Green's function in this case has simple poles in the lower half plane of the complex frequency plane which are associated with the so-called resonant states [44]. The residuum at the resonant frequency ω_r can be obtained by analyzing the behavior of the Green's function in the vicinity of the pole. Using the approach of Ref. [45], we assume that for $\omega \approx \omega_r$

$$\mathbf{G}(z, z'; \omega, \boldsymbol{k}) = \frac{\mathbf{C}_r(z, z'; \boldsymbol{k})}{\omega^2 - \omega_r^2} + \mathbf{M}_r(z, z'; \omega, \boldsymbol{k}), \tag{8}$$

where both $\mathbf{C}_r$ and $\mathbf{M}_r$ are piecewise, twice-differentiable functions of z and z' and $\mathbf{M}_r$ is an analytic function of ω. In order to use the generalized Green's formula we also have to introduce the adjoint operator and adjoint Green's function [46]:

$$\hat{\boldsymbol{\mathcal{L}}}^\dagger(z; \omega, \boldsymbol{k})\mathbf{G}^\dagger(z, z'; \omega, \boldsymbol{k}) = \delta(z - z')\boldsymbol{\sigma}_0, \tag{9}$$

where

$$\hat{\boldsymbol{\mathcal{L}}}^\dagger = (\partial_z + \mathbf{A}^T)(\partial_z + \mathbf{A}) - \mathbf{B}^T + k_0^2\mathbf{B}_0, \tag{10}$$

with the identical boundary conditions as given by Eq. (7) for $\boldsymbol{G}(z, z')$. In this case, according to the reciprocity theorem, we have

$$\hat{\boldsymbol{\mathcal{L}}}^\dagger(z'; \omega, \boldsymbol{k})\mathbf{G}^T(z, z'; \omega, \boldsymbol{k}) = \delta(z - z')\boldsymbol{\sigma}_0. \tag{11}$$

It can be shown that (see Appendix A)

$$\mathbf{C}_r(z, z') = \boldsymbol{u}_r(z)\boldsymbol{w}_r^T(z'), \tag{12}$$

where $\boldsymbol{u}_r(z)$ and $\boldsymbol{w}_r(z')$ are the resonant solutions of two coupled equations,

$$\left((\partial_z - \mathbf{A}^T)(\partial_z - \mathbf{A}) - \mathbf{B} + \frac{\omega_r^2}{c^2}\mathbf{B}_0\right)\boldsymbol{u}_r(z) = \mathbf{0}, \tag{13a}$$

$$\left((\partial_z + \mathbf{A}^T)(\partial_z + \mathbf{A}) - \mathbf{B}^T + \frac{\omega_r^2}{c^2}\mathbf{B}_0\right)\boldsymbol{w}_r(z) = \mathbf{0}, \tag{13b}$$

with outgoing wave boundary conditions

$$\partial_z \boldsymbol{u}_r(z) = \pm ik_{zr}\boldsymbol{u}_r(z), \quad \partial_z \boldsymbol{w}_r(z) = \pm ik_{zr}\boldsymbol{w}_r(z), \tag{14}$$

where $k_{zr} = \sqrt{\varepsilon_a\omega_r^2/c^2 - k^2}$. Applying the generalized Green's formula and taking into account the boundary

conditions, we get the normalization for $\boldsymbol{u}_r$ and $\boldsymbol{w}_r$:

$$\frac{1}{c^2}\int_a^b \boldsymbol{w}_r^T(z)\mathbf{B}_0(z)\boldsymbol{u}_r(z)dz$$
$$+ \frac{in_a^2}{2c^2 k_{zr}}\big(\boldsymbol{w}_r^T(b)\boldsymbol{u}_r(b) + \boldsymbol{w}_r^T(a)\boldsymbol{u}_r(a)\big) = 1. \qquad (15)$$

The principal part of the Green's function in the vicinity of the resonant value ω_r is therefore given by

$$\mathbf{G}(z,z';\omega,\boldsymbol{k}) \approx \frac{\boldsymbol{u}_r(z)\boldsymbol{w}_r^T(z')}{2\omega_r(\omega - \omega_r)}. \qquad (16)$$

Equations (4) and (10) have parity ($\mathcal{P}$) and time ($\mathcal{T}$) symmetries, and can be considered foundations of optical simulations of $\mathcal{PT}$-symmetric quantum mechanics [47].

III. SCATTERING AT FINITE ANGLE: A PERTURBATIVE APPROACH

Solving the equation for resonant states $\boldsymbol{u}_r$ or $\boldsymbol{w}_r$,

$$\hat{\mathcal{L}}(z;\omega_r,\boldsymbol{k})\boldsymbol{u}_r(z) = 0, \qquad (17)$$

with outgoing wave boundary conditions would provide the dispersion relation $\omega_r(\boldsymbol{k})$ giving the information about the frequency and lifetimes of resonant modes for each direction of the outgoing wave characterized by the in-plane vector $\boldsymbol{k}$. Nevertheless, exact calculation of resonant conditions is time consuming because it requires solving Eq. (17) for each vector $\boldsymbol{k}$ separately. The other method is to find the resonant states only for perpendicular incidence $\boldsymbol{k} = 0$ and deduce resonant states for $\boldsymbol{k} \neq 0$ using the perturbation method. We therefore introduce a zero-order operator, which for a given $\boldsymbol{k}$ is given by

$$\hat{\mathcal{L}}_0(z;\omega,\boldsymbol{k}) = \partial_z^2 + \left(\frac{\omega^2}{c^2} - \frac{k^2}{n_a^2}\right)\mathbf{B}_0(z). \qquad (18)$$

The resonant solutions $\overset{o}{\boldsymbol{u}}_r$ are in this case obtained from the equation

$$\left(\partial_z^2 + \frac{\overset{o}{\omega}_r^2(0)}{c^2}\mathbf{B}_0(z)\right)\overset{o}{\boldsymbol{u}}_r(z) = 0, \qquad (19)$$

while the $\boldsymbol{k}$-dependent, "unperturbed" resonant frequencies are given by the relation $\overset{o}{\omega}_r^2(\boldsymbol{k}) = \overset{o}{\omega}_r^2(0) + c^2 k^2/n_a^2$. Note that the perturbation defined as $\hat{\mathcal{L}}' = \hat{\mathcal{L}} - \hat{\mathcal{L}}_0$ is different from zero only in the region of the cavity and mirrors and is ω independent:

$$\hat{\mathcal{L}}'(z) = -\mathbf{A}^T\partial_z - \partial_z\mathbf{A} + \mathbf{A}^T\mathbf{A} - \mathbf{B} + \frac{k^2}{n_a^2}\mathbf{B}_0. \qquad (20)$$

This is because outside the cavity $\mathbf{B} = k^2\boldsymbol{\sigma}_0$ while $\mathbf{B}_0 = n_a^2\boldsymbol{\sigma}_0$. In our approach we are looking for the resonant solutions $\boldsymbol{u}_m$ in the form of a linear combination of the unperturbed resonance functions $\overset{o}{\boldsymbol{u}}_n$:

$$\boldsymbol{u}_m(z) = \sum_n \frac{a_{nm}}{\sqrt{\overset{o}{\omega}_n(\boldsymbol{k})}}\overset{o}{\boldsymbol{u}}_n(z). \qquad (21)$$

Representing the Green's functions as sums over simple poles associated with the resonant states according to the Mittag-Leffler theorem [48], we obtained an eigenequation for the nth column of the a_{mn} matrix:

$$\omega_n(\boldsymbol{k})a_{mn} = \sum_p \left(\overset{o}{\omega}_m(\boldsymbol{k})\delta_{mp} - \frac{(\hat{\mathcal{L}}')_{mp}}{2\sqrt{\overset{o}{\omega}_m(\boldsymbol{k})\overset{o}{\omega}_p(\boldsymbol{k})}}\right)a_{pn}. \qquad (22)$$

We discuss the details in Appendix B.

Typically the sum over p can be limited to only a few modes in the energy region of interest so Eq. (22) can be written as an eigenvalue problem for some effective, non-Hermitian Hamiltonian (here we drop the column index n in a_{mn}):

$$\sum_p \mathcal{H}_{mp}(\boldsymbol{k})a_p = \omega(\boldsymbol{k})a_m, \qquad (23)$$

where

$$\mathcal{H}_{mp}(\boldsymbol{k}) = \left(\overset{o}{\omega}_m(\boldsymbol{k})\delta_{mp} - \frac{(\hat{\mathcal{L}}')_{mp}}{2\sqrt{\overset{o}{\omega}_m(\boldsymbol{k})\overset{o}{\omega}_p(\boldsymbol{k})}}\right). \qquad (24)$$

Since the resulting Hamiltonian is $\mathcal{PT}$-symmetric we expect to observe so-called exceptional points in k space, where real and imaginary parts of $\omega(\mathbf{k})$ both coalesce.

We considered so far light transmission through a cavity slab composed of a birefringent layer extending from $z = 0$ to $z = L$ encompassed on both sides by distributed Bragg reflectors (DBRs) in a form of multilayer structures so that the whole system was contained between $z = a < 0$ and $z = b > L$. As we have already mentioned, the analysis of resonances for various angles of light incidence in the birefringent cavity, i.e., for various values of $\boldsymbol{k}$, was based on the properties of the resonant states at $\boldsymbol{k} = 0$. Such states can be fairly easily obtained using standard numerical methods, e.g., the transfer matrix technique or recursive Green's function method. However, in order to get a better understanding of the nature of the resonant modes, we proposed to adopt a model which could be solved analytically. Similarly, as it is often discussed in the course of quantum mechanics, we replaced the semipermeable DBRs with very thin barrier layers made of an artificial dielectric material of very high dielectric permeability (see Appendix F 1). In the limit of infinitely thin barriers and for perpendicular light incidence we obtained the simple equation for the electric field,

$$\left(\partial_z^2 + \tilde{n}_s^2(z)\frac{\omega^2}{c^2}\right)\boldsymbol{E}_s(z) = \boldsymbol{0}, \qquad (25)$$

where $\tilde{n}_s^2(z) = \Theta(L - z)\Theta(z)(n_s^2 - n_a^2) + n_a^2 - 2\zeta_s c^2(\delta(z) + \delta(z - L))/\omega^2$ [see Fig. 2(b)]. Here $n_s = \sqrt{\varepsilon_{ss}}$ denotes the refractive index of the material inside the cavity for the horizontal ($s = X$, along the x axis) and vertical ($s = Y$, along the y axis) polarization of light, respectively. The strength of the δ-like mirrors is represented by the parameter ζ_s separately for each polarization. The electric field of the mth mode with polarization s normalized according to Eq. (15) inside the cavity is given by

$$\boldsymbol{E}_{sm}(z) = \boldsymbol{E}_{0,sm}\sin(\kappa_{sm}(z - d_{sm})), \qquad (26)$$

where the complex wave number κ_{sm} is found from the implicit equation

$$\kappa_{sm} = -\frac{i}{L}\ln\left(\frac{1 - i\frac{(n_a+n_s)\kappa_{sm}}{2\zeta_s n_s}}{1 - i\frac{(n_a-n_s)\kappa_{sm}}{2\zeta_s n_s}}\right) + \frac{m\pi}{L}, \qquad (27)$$

and $d_{sm} = \Delta_{sm}L/2\kappa_{sm}$ describes the penetration depth of electromagnetic modes outside the cavity and is similar to scattering length from nuclear physics. Here, $\Delta_{sm} = \kappa_{sm} - m\pi/L$ denotes a usually small deviation of κ_{sm} from the perfect Fabry-Pérot value $m\pi/L$ [16]. The frequency of the resonant mode sm is $\omega_{sm} = c\kappa_{sm}/n_s$. Note that for very good reflectors, i.e., in the limit $|\zeta_s| \to \infty$, we have $\Delta_{sm} \to 0$. The solutions of Eq. (27) generally depend on the dispersions of refractive indices and ζ_s. Assuming for example that n_a, n_s, and ζ_s are independent of frequency, and expanding Eq. (27) to the second order in $1/\zeta_s$, we obtain an approximate solution which is valid for large ζ_s:

$$\kappa_{sm} \approx \frac{m\pi}{L} - \frac{m\pi}{L^2\zeta_s} + \frac{m\pi}{L^3\zeta_s^2} - i\frac{n_a m^2\pi^2}{2L^3 n_s \zeta_s^2}, \qquad (28)$$

so in this case

$$\Delta_{sm} \approx -\frac{m\pi}{L^2\zeta_s}\left(1 - \frac{1}{L\zeta_s}\left(1 - i\frac{n_a m\pi}{2n_s}\right)\right). \qquad (29)$$

Note that in general Δ_{sm} depends on the polarization s in this model. The actual dependence of ζ_s on frequency can be adjusted to reflect the properties of the real mirror structure.

A. Effective multimode Hamiltonian

If the dielectric tensor inside the cavity is position independent, the matrix elements of the effective Hamiltonian in Eq. (24) can be expressed in terms of simple, normalized overlap integrals which, to the lowest order in Δ_{sm}, are given by

$$P_{sm,s'm'} = \frac{n_s n_{s'}}{c^2}\int_0^L (\boldsymbol{E}_{sm}(z))^T \boldsymbol{E}_{s'm'}(z)\,dz$$

$$\approx \begin{cases} 0 & \text{if } m+m' \text{ is odd} \\ 1 & \text{if } m = m' \\ \frac{2L(m'\Delta_{sm}-m\Delta_{s'm'})}{\pi(m^2-m'^2)} & \text{in other cases,} \end{cases} \qquad (30)$$

and

$$Q_{sm,s'm'} = \frac{n_s n_{s'}}{c^2}\int_0^L (\boldsymbol{E}_{sm}(z))^T \partial_z \boldsymbol{E}_{s'm'}(z)\,dz$$

$$\approx \begin{cases} 0 & \text{if } m+m' \text{ is even} \\ \frac{4mm'}{L(m^2-m'^2)} + \frac{8(m^3\Delta_{s'm'}-m'^3\Delta_{sm})}{\pi(m^2-m'^2)^2} & \text{if } m+m' \text{ is odd.} \end{cases} \qquad (31)$$

The integral $P_{sm,s'm'}$ is proportional to the overlap between the modal electric fields, and the integral $Q_{sm,s'm'}$ is proportional to the overlap between electric field and its derivative as in Eq. (20). The Hamiltonian matrix element is then given by

$$\mathcal{H}_{sm,s'm'} = \delta_{ss'}\delta_{mm'}\overset{o}{\omega}_{sm}(\boldsymbol{k}) + \chi_{sm,s'm'}$$
$$\times\left((\mathbf{A}_1)_{ss'}Q_{sm,s'm'} + \left(\mathbf{B}_1 - \frac{k^2}{n_a^2}\mathbf{B}_0\right)_{ss'}P_{sm,s'm'}\right), \qquad (32)$$

where $\chi_{sm,s'm'} = c^2/2n_s n_{s'}\sqrt{\overset{o}{\omega}_{sm}\overset{o}{\omega}_{s'm'}}$, $\mathbf{A}_1 = \mathbf{A} + \mathbf{A}^T$, and $\mathbf{B}_1 = \mathbf{B} - \mathbf{A}^T\mathbf{A}$. We will refer to Eq. (32) as the multimode Hamiltonian, since the solution depends on the overlaps with a set of optical modes. More modes used for the calculation give better accuracy, especially in simulations of correct polarization patterns, at the cost of increasing computational time.

B. Two-mode Hamiltonian

In the general case the eigenmodes for $k \neq 0$ are obtained by solving the system of equation

$$\sum_{s'=X,Y}\sum_{m'}(\mathcal{H}_{sm,s'm'} - \omega\delta_{ss''}\delta_{mm'})a_{s'm'} = 0, \qquad (33)$$

where the summation is carried over the infinite number of resonant modes. In practice, however, it is adequate to include only a finite number of modes and the range of summation depends on the range of interest. In particular we can consider just two modes which are degenerate or nearly degenerate at $\boldsymbol{k} = 0$. The contribution from the other modes to such a limited 2×2 matrix problem can be included using the perturbation theory. Importantly, since in our approximation we only consider terms quadratic in $\boldsymbol{k}$ we should include the linear terms in $\hat{\mathcal{L}}'$ in the second order of the perturbation theory while all the other terms are included in the lowest order. We therefore split the Hamiltonian matrix into three parts, in which the first term is diagonal and the other two, multiplied by the coupling constant λ, are treated as perturbation:

$$\mathcal{H}_{sm,s'm'} = \mathcal{H}^{(0)}_{sm,s'm'} + \lambda\left(\mathcal{H}^{(1)}_{sm,s'm'} + \mathcal{H}^{(2)}_{sm,s'm'}\right), \qquad (34)$$

where

$$\mathcal{H}^{(0)}_{sm,s'm'} = \delta_{ss'}\delta_{mm'}\overset{o}{\omega}_{sm}(\boldsymbol{k}), \qquad (35a)$$

$$\mathcal{H}^{(1)}_{sm,s'm'} = \chi_{sm,s'm'}(\mathbf{A}_1)_{ss'}Q_{sm,s'm'}, \qquad (35b)$$

$$\mathcal{H}^{(2)}_{sm,s'm'} = \chi_{sm,s'm'}\left(\mathbf{B}_1 - \frac{k^2}{n_a^2}\mathbf{B}_0\right)_{ss'}P_{sm,s'm'}. \qquad (35c)$$

Similarly to the Foldy-Wouthuysen method [49], we divide all modes into two blocks: a group of states of interest and all the other states. We then apply a transformation of basis that eliminates from the Hamiltonian matrix the coupling elements between these two blocks (at least up to second order in $\boldsymbol{k}$). The modified Hamiltonian matrix $\mathcal{H}'_{sm,s'm'}$ becomes

$$\mathcal{H}'_{sm,s'm'} = \mathcal{H}_{sm,s'm'} + \frac{1}{2}\sum_{s''m''}{}' \mathcal{H}^{(1)}_{sm,s''m''}\mathcal{H}^{(1)}_{s''m'',s'm'}$$
$$\times\left(\frac{1}{\overset{o}{\omega}_{sm} - \overset{o}{\omega}_{s''m''}} + \frac{1}{\overset{o}{\omega}_{s'm'} - \overset{o}{\omega}_{s''m''}}\right). \qquad (36)$$

This expression, limited to the subspace spanned by two nearly degenerate modes, gives rise to the two-mode Hamiltonian. Note that $\mathcal{H}^{(1)}_{sm,s''m''}$ is linear in $\boldsymbol{k}$ so our procedure resembles the $\boldsymbol{k} \cdot \boldsymbol{p}$ method widely used to describe the band structure in semiconductors. Here we approximated the resonant frequencies in the denominators $\overset{o}{\omega}_{s'm'}(\boldsymbol{k}) \approx \overset{o}{\omega}_{s'm'}(0) \equiv \overset{o}{\omega}_{s'm'}$ and the summation is carried over all states outside the group of interest. Using this method we can generate the effective 2×2 Hamiltonian matrices for three interesting cases.

Our two-mode Hamiltonian matrix corresponds to the perturbed, i.e., rotated basis, set, so the expression for each Stokes polarization parameter of light has to be modified accordingly. The relation between the perturbed and unperturbed basis states is assumed to be of the form

$$E'_{s'm'}(z) = \sum_{sm} (e^{\hat{R}})_{sm,s'm'} E_{sm}(z),$$ (37)

where $E'_{s'm'}$ and E_{sm} are perturbed and unperturbed basis states, respectively. The coefficients of the matrix $\hat{R}$ in the linear order with respect to $\mathcal{H}^{(1)}_{sm,s'm'}$ [Eq. (35b)] are

$$R_{sm,s'm'} = \begin{cases} -\dfrac{\mathcal{H}^{(1)}_{sm,s'm'}}{\overset{o}{\omega}_{sm} - \overset{o}{\omega}_{s'm'}} & \text{if (1)} \\ 0 & \text{if (2),} \end{cases}$$ (38)

where (1) denotes the case in which E_{sm} and $E_{s'm'}$ belong to different subsets of the basis set and (2) denotes the opposite case. This additional rotation of basis is crucial for proper description of polarization of optical eigenmodes. The form of the two-mode Hamiltonian in Eq. (36), even though it includes the contribution from the other states, does not contain enough information to represent accurately the polarization of optical eigenmodes. The formulas to calculate Stokes polarization parameters, including the rotation of basis, are presented in Appendix E.

IV. RESULTS FOR TWO-MODE HAMILTONIAN

A. General information

We consider a general birefringent system where one of the optical axes (ordinary or extraordinary) is parallel to the y axis. For instance, it can be a cavity filled with a liquid crystal, where the molecules can rotate in the x-z plane, as in Refs. [15,16,23,26,33,35,43]. Such a birefringent system is characterized by the following dielectric tensor:

$$\hat{\varepsilon} = \hat{\varepsilon}^T = \begin{bmatrix} \varepsilon_{xx} & 0 & \varepsilon_{xz} \\ 0 & \varepsilon_{yy} & 0 \\ \varepsilon_{zx} & 0 & \varepsilon_{zz} \end{bmatrix},$$ (39)

where ε_{ij} can be smoothly tuned in a wide range of values leading to three regimes of nearly coupled pairs of modes:

(i) $X(m+1)$ and $Y(m)$ is the regime of the modes of opposite parity [16,23,26,43] [see Fig. 3(b)] for which the dispersion relation obtained by diagonalization of the effective 2×2 Hamiltonian matrix is presented in Fig. 3(a).

(ii) $X(m+2)$ and $Y(m)$ is the regime of the modes of the same parity [33,35] [see Figs. 3(c) and 3(d)].

(iii) $X(m)$ and $Y(m)$ is the regime of the modes of the same mode number m and horizontal (X) and vertical (Y) linear polarization [15,33,36] [see Figs. 3(e) and 3(f)].

In each subsequent simulation, we used parameter values for three different regimes according to recent experiments [16,18,26,33,35,43] listed in Table I. We limited the summation over the intermediate states with mode numbers m from 5 to 23 ($X(m)$, $Y(m)$), 24 ($X(m+1)$, $Y(m)$), and 25 ($X(m+2)$, $Y(m)$), keeping the same number of nine modes below and above the resonance around the chosen mode $Y(m = 14)$. We kept the cavity thickness $L = 3$ μm, the strength of the δ-
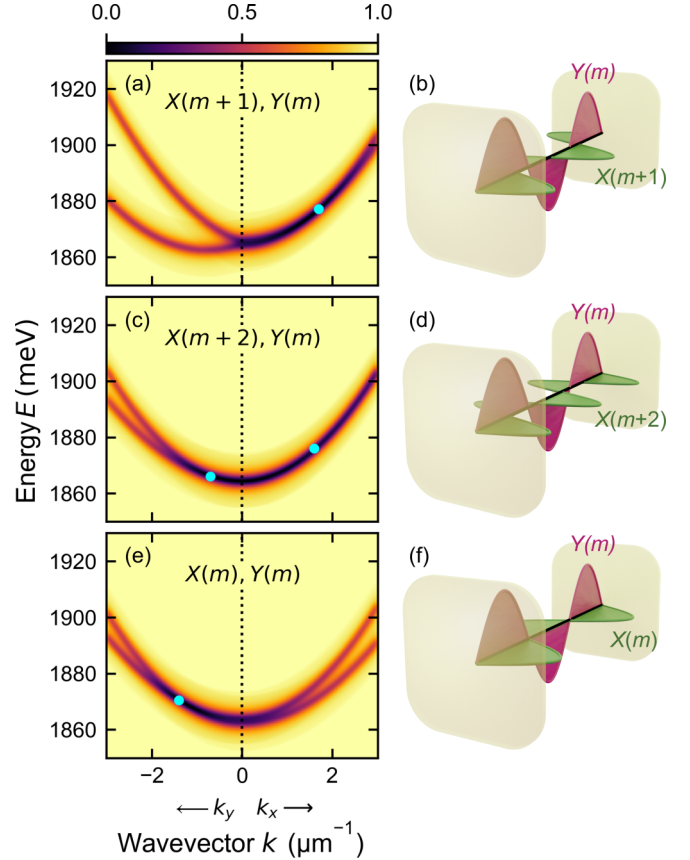

FIG. 3. [(a), (c), (e)] Dispersion relation in k_y and k_x directions (left and right parts of each figure, respectively) for three different possible regimes in a birefringent liquid crystal [(b), (d), (f)] obtained by diagonalization of two-mode effective Hamiltonian matrices: (a) Eq. (45), (c) Eq. (47), and (e) Eq. (49). The cyan circle marks the crossing between two energy branches. Schematic idea of three different couplings in cavity: (b) $X(m+1)$, $Y(m)$; (d) $X(m+2)$, $Y(m)$; and (f) $X(m)$, $Y(m)$.

like mirrors $\zeta_X = 39$ μm^{-1}, $\zeta_Y = 40$ μm^{-1}, and the refractive index outside the cavity, $n_a = 1$.

The results of the two-mode approximation for each possible regime in the birefringent microcavity are obtained by diagonalization of the effective 2×2 Hamiltonian matrices, which have following form:

$$\mathcal{H}' = \begin{bmatrix} h_0 + h_z & h_x - ih_y \\ h_x + ih_y & h_0 - h_z \end{bmatrix}$$

$$= h_0 \boldsymbol{\sigma}_0 + h_x \boldsymbol{\sigma}_x + h_y \boldsymbol{\sigma}_y + h_z \boldsymbol{\sigma}_z,$$ (40)

TABLE I. Values of each parameter for three different regimes of cavity modes used in all simulations.

	$X(m)Y(m)$	$X(m+1)Y(m)$	$X(m+2)Y(m)$
ε_{xx}	2.3739	2.7861	3.1279
ε_{yy}	2.3685	2.3685	2.3685
ε_{zz}	3.2346	2.8224	2.4806
$\varepsilon_{xz} \times 10$	0.6814	4.3536	2.9177

where $\boldsymbol{\sigma}_0$, $\boldsymbol{\sigma}_x$, $\boldsymbol{\sigma}_y$, and $\boldsymbol{\sigma}_z$ are Pauli matrices and all h_i coefficients are complex functions of $\boldsymbol{k}$ of linear or quadratic order. For each regime we present the Stokes polarization parameters, taking into account the additional transformation of basis according to Eqs. (37) and (38). For comparison we also include results of Stokes polarization parameters without additional transformation of basis, which was typically omitted by other authors.

For each case, we observe the $\boldsymbol{k}$-dependent coupling between two modes. We denote by E_+ and E_- the energy of the upper and lower energy branches, respectively, so that, for each $\boldsymbol{k}$, $\mathrm{Re}(E_+(\boldsymbol{k})) \geqslant \mathrm{Re}(E_-(\boldsymbol{k}))$, where $E_\pm$ are eigenvalues of the general effective 2×2 Hamiltonian matrix in Eq. (40) equal to

$$E_\pm = h_0 \pm \sqrt{h_x^2 + h_y^2 + h_z^2}. \tag{41}$$

For the Hermitian Hamiltonian the equality of energies occurs at the Dirac points, which in the non-Hermitian system turn into the diabolical or exceptional points as an effect of losses [35,36,50,51]. The condition for degeneracy points is given by the following equation:

$$h_x^2 + h_y^2 + h_z^2 = 0. \tag{42}$$

In the case of Hermitian Hamiltonians h_x, h_y, h_z are real, implying that they all vanish at the degeneracy points. It follows that, when

$$\boldsymbol{\mathcal{H}}' - E_\pm \boldsymbol{\sigma}_0 = h_x \boldsymbol{\sigma}_x + h_y \boldsymbol{\sigma}_y + h_z \boldsymbol{\sigma}_z = \mathbf{0}, \tag{43}$$

there exist two linearly independent eigenvectors at each such so-called diabolical point. At the degeneracy point of a non-Hermitian Hamiltonian at least two h_i coefficients can be different from zero and there exists only one eigenvector. In such a case we are dealing with an exceptional point. In fact, upon a small change of parameters preserving condition (42), the diabolical points can spawn into a pair of exceptional points with mutually orthogonal eigenvectors [52]. In the general case all parameters are complex numbers, but usually one part (real or imaginary) of h_x and h_y is much smaller than the other. In the first approximation we only consider the dominant parts (real or imaginary) denoted by h_x' and h_y', while h_z is taken in the form $h_z = h_z' + ih_z''$, where $h_z' = \mathrm{Re}(h_z)$ and $h_z'' = \mathrm{Im}(h_z)$. In addition, we assumed that $h_z'' \neq 0$ in the analyzed region of $\boldsymbol{k}$. Using these simplifications, Eq. (42) can be rewritten as

$$(h_x')^2 + (h_y')^2 - (h_z'')^2 = 0, \tag{44a}$$

$$h_z' = 0. \tag{44b}$$

For each regime we can obtain different solutions presented in the next sections.

B. The regime of modes of opposite parity, $X(m+1)$ and $Y(m)$: Photonic Rashba-Dresselhaus spin-orbit coupling

Photonic Rashba-Dresselhaus spin-orbit coupling takes place when $(m+1)/n_X \approx m/n_Y$ (where $n_X = \sqrt{\overset{o}{\varepsilon}_{xx}}$ and $n_Y = \sqrt{\overset{o}{\varepsilon}_{yy}}$), i.e., for $\overset{o}{\omega}_{X(m+1)} \approx \overset{o}{\omega}_{Y(m)}$ [see Figs. 3(a) and 3(b)]. The
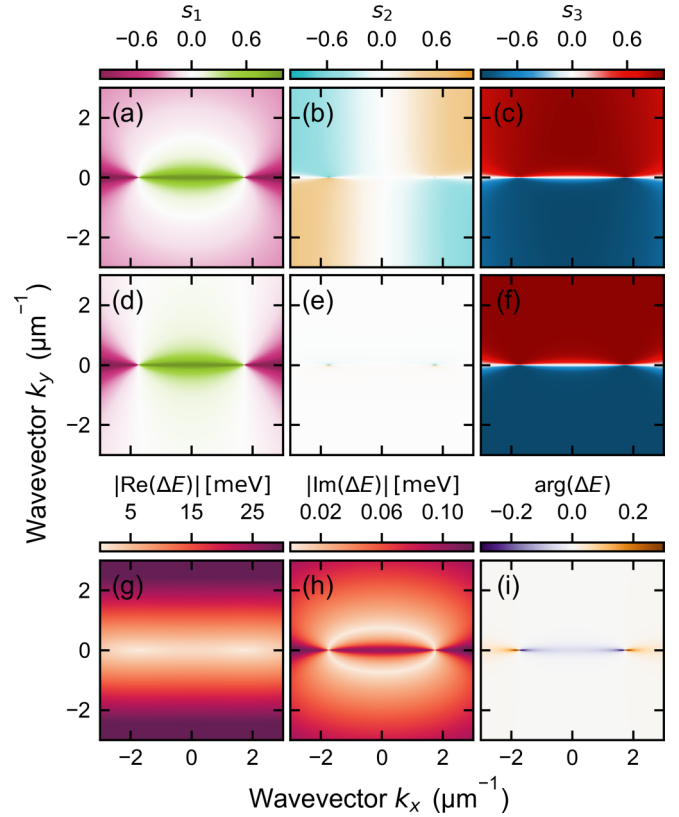

FIG. 4. Rashba-Dresselhaus $X(m+1)$, $Y(m)$ regime. Stokes polarization parameters [(a) and (d)] s_1, [(b) and (e)] s_2, and [(c) and (f)] s_3 for upper energy branch in $\boldsymbol{k}$ space. The Stokes polarization parameters in (a)–(c) were calculated including additional rotation of basis (see Appendix E) and in (d)–(f) they were calculated without taking into account additional rotation of basis. [(g)–(i)] The absolute values of real and imaginary parts and the phase of difference between two eigenvalues of Hamiltonian (45), $\Delta E = E_+ - E_-$.

effective two-mode Hamiltonian takes the form

$$\boldsymbol{\mathcal{H}}' = \left(\omega_0 + i\Gamma_0 + \frac{\hbar k_x^2}{2m_x} + \frac{\hbar k_y^2}{2m_y}\right)\boldsymbol{\sigma}_0$$
$$+ (\Delta + i\delta\Gamma + \delta_x k_x^2 + \delta_y k_y^2)\boldsymbol{\sigma}_z - 2\alpha k_y\boldsymbol{\sigma}_y, \tag{45}$$

where m_x and m_y are effective masses of the cavity photons, α is the optical Rashba-Dresselhaus spin-orbit coupling constant [16], coefficients Δ, δ_x, and δ_y are parameters that appeared as a result of the birefringence in the system, and $\delta\Gamma$ corresponds to the difference between values of ζ_X and ζ_Y, i.e., the difference in reflectivities of mirrors for two orthogonal polarizations. The formula for the modified Hamiltonian matrix in Eq. (36) can be used to calculate all parameters in Eq. (45) and the results are presented as Eq. (C4). Simplified versions of this Hamiltonian derived for a perfect cavity (built of perfect impenetrable mirrors) were considered in Refs. [16–21,26].

Figure 4 shows results obtained by diagonalization of the two-mode Hamiltonian (45). Figures 4(a)–4(f) present Stokes polarization parameters for the upper energy branch in $\boldsymbol{k}$ space, but in Figs. 4(a)–4(c) we calculated Stokes polarization parameters (Appendix E), which include the effect of additional rotation of basis, while in Figs. 4(d)–4(f) we did not

take into account this effect. Neglecting these modifications would lead to the vanishing of s_2 [see Figs. 4(b) and 4(e)] and change the behavior s_1 component in such a way that it would not change its sign in the k_y direction [see Figs. 4(a) and 4(d)].

Thanks to the analytic form of the two-mode Hamiltonian we could derive conditions for the existence of topological points in **k** space. The degeneracy of real [see Fig. 4(g)] and imaginary [see Fig. 4(h)] parts of energy occurs along four Fermi arcs connected by four exceptional points [see Fig. 4(i)] at which we observe degeneracy of both parts of the energy. In this regime $\delta_x < 0$, $h'_x = 0$, $h'_y = -2\alpha'$, $h'_z = \Delta + \delta'_x k_x^2 + \delta'_y k_y^2$, and $h''_z = \delta\Gamma$, where $x' = \text{Re}(x)$, so solving Eq. (44) yields the following formula for positions of these points:

$$k_{e,x} = \pm\sqrt{-\frac{4\Delta(\alpha')^2 + \delta'_y \delta\Gamma^2}{4\delta'_x(\alpha')^2}} \xrightarrow{\Delta \gg \delta\Gamma}$$

$$\pm\sqrt{-\frac{\Delta}{\delta'_x}\left(1 + \frac{\delta'_y \delta\Gamma^2}{8(\alpha')^2\Delta}\right)}, \qquad (46a)$$

$$k_{e,y} = \pm\frac{\delta\Gamma}{2\alpha'}. \qquad (46b)$$

In the first approximation the k_y component of position of the exceptional points depends on the difference between losses for two orthogonal modes, and is independent of the detuning Δ. At the same time the k_x component of position of the exceptional points depends on the detuning $\sqrt{-\Delta/\delta'_x}$, so we may smoothly vary position in this direction as long as exceptional points exist.

C. The regime of modes of the same parity: $X(m+2)$ and $Y(m)$

In the case of almost degenerate modes of the same parity with different mode number, such as $X(m+2)$ and $Y(m)$, for which $(m+2)/n_X \approx m/n_Y$, i.e., for $\overset{o}{\omega}_{X(m+2)} \approx \overset{o}{\omega}_{Y(m)}$ [see Figs. 3(c) and 3(d)], there is no direct linear coupling in **k** and the effective Hamiltonian has the form

$$\mathcal{H}' = \left(\omega_0 + i\Gamma_0 + \frac{\hbar k_x^2}{2m_x} + \frac{\hbar k_y^2}{2m_y}\right)\boldsymbol{\sigma}_0 - 2\beta k_x k_y \boldsymbol{\sigma}_x$$

$$+ \left(\Delta + i\delta\Gamma + \delta_x k_x^2 + \delta_y k_y^2\right)\boldsymbol{\sigma}_z - 2i\gamma k_x k_y \boldsymbol{\sigma}_y, \qquad (47)$$

where m_x and m_y are effective masses of a photon in a cavity, coefficients Δ, δ_x, δ_y, and γ are parameters that appeared as a result of the birefringence in the system, β comes from the coupling with other optical modes, and $\delta\Gamma$ is induced by the difference between the values of ζ_X and ζ_Y, i.e., the difference in reflectivities of mirrors for two orthogonal polarizations. We used the formula for a modified Hamiltonian matrix [Eq. (36)] to calculate all parameters of Hamiltonian (47) and the results are given in Eq. (C6) in Appendix C 2.

Note that in the limit of perfect mirrors, i.e., in the limit $|\zeta_s| \to \infty$, we have $\Delta_{sm} \to 0$ and $P_{X(m+2),Y(m)} \to 0$ [Eq. (30)], and the coefficient $\gamma \to 0$. Thus the term proportional to $\boldsymbol{\sigma}_y$ in this Hamiltonian [Eq. (47)] is also negligibly
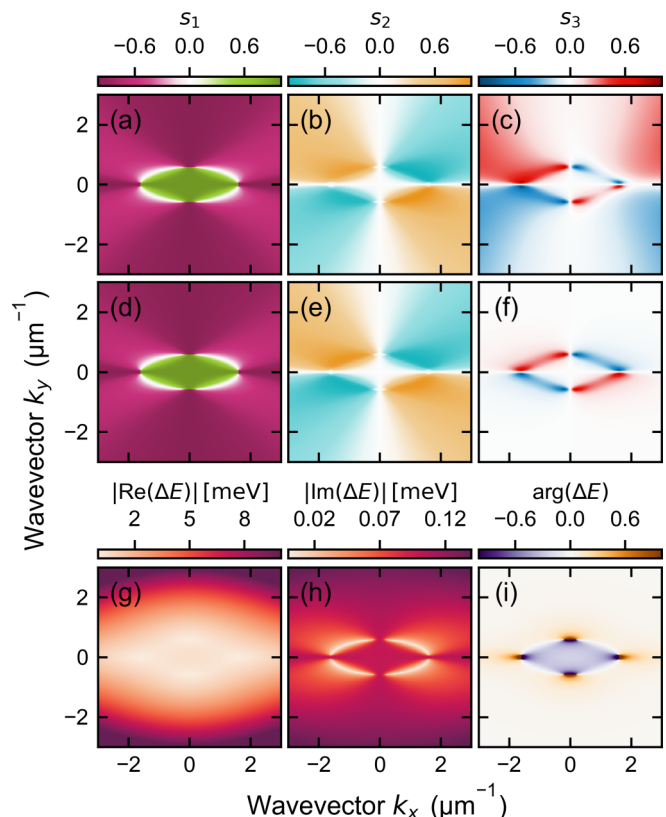

FIG. 5. The same-parity $X(m+2)$, $Y(m)$ regime. Stokes polarization parameters [(a) and (d)] s_1, [(b) and (e)] s_2, and [(c) and (f)] s_3 for upper energy branch in **k** space. The Stokes polarization parameters in (a)–(c) were calculated including additional rotation of basis (see Appendix E) and in (d)–(f) they were calculated without taking into account additional rotation of basis. [(g)–(i)] The absolute values of real and imaginary parts and the phase of difference between two eigenvalues of Hamiltonian (47), $\Delta E = E_+ - E_-$.

small. The coefficient β is dominated by the contribution from the quadratic corrections and is responsible for the coupling between two polarizations.

Figure 5 presents the results of diagonalization of the two-mode Hamiltonian [Eq. (47)]. Figures 5(a)–5(f) show Stokes polarization parameters for the upper energy branch in **k** space taking into account the additional rotation of basis [see Figs. 5(a)–5(c) and Appendix E] and without these additional corrections [see Figs. 5(d)–5(f)]. Ignoring the additional rotation of basis would lead to a nonphysical result, namely, vanishing of the s_3 Stokes polarization parameter for large value of **k** [see Figs. 5(c) and 5(f)]. The s_1 and s_2 Stokes polarization parameters are well reproduces without including rotation of basis [see Figs. 5(a) and 5(d) for the s_1 Stokes polarization component, and Figs. 5(b) and 5(e) for the s_2 Stokes polarization component).

The simple version of the two-mode Hamiltonian [Eq. (47)] allows us to derive the expressions for the position of topological points in **k** space (exceptional points). In this regime the degeneracy of real [Fig. 5(g)] and imaginary [Fig. 5(h)] parts of the energy exist along eight Fermi arcs, which are connected by eight exceptional points [Fig. 5(i)] [35], at which we observe degeneracy of both parts of

the energies. Solving Eq. (44) with $h'_x = -2\beta' = -2\mathrm{Re}(\beta)$, $h'_y = -2i\gamma' = -2i\mathrm{Re}(\gamma)$, $h'_z = \Delta + \delta'_x k_x^2 + \delta'_y k_y^2$, and $h''_z = \delta\Gamma$, where $\delta'_x = \mathrm{Re}(\delta_x)$ and $\delta'_y = \mathrm{Re}(\delta_y)$, yields the following formulas for positions of exceptional points:

$$k_{e,x} = \pm \sqrt{-\frac{\Delta \pm \sqrt{\Delta^2 - \frac{\delta\Gamma^2 \delta'_x \delta'_y}{(\beta')^2 - (\gamma')^2}}}{2\delta'_x}}, \quad (48a)$$

$$k_{e,y} = \pm \sqrt{\frac{-\Delta \pm \sqrt{\Delta^2 - \frac{\delta\Gamma^2 \delta'_x \delta'_y}{(\beta')^2 - (\gamma')^2}}}{2\delta'_y}}. \quad (48b)$$

In this regime $\delta'_x < 0$, $\delta'_y < 0$, $\beta' < 0$, $\gamma' > 0$, and $|\beta'| > |\gamma'|$ so for $\Delta^2 > \delta\Gamma^2 \delta'_x \delta'_y / ((\beta')^2 - (\gamma')^2)$ we observe eight exceptional points. The k_x and k_y components depend on the detuning, so we can smoothly change the position of each of these points as long as they exist, because if $\Delta^2 = \delta\Gamma^2 \delta'_x \delta'_y / ((\beta')^2 - (\gamma')^2)$ the exceptional points with different winding number ($\pm 1/2$) meet and eventually annihilate [35]. As shown in Figs. 5(a) and 5(g) the position of Fermi arcs for the real part of the energy is related to the abrupt change of the s_1 Stokes polarization parameter. A similar case exists for Fermi arcs for the imaginary part of the energy, because their positions are related to local maxima of s_2 Stokes polarization parameters [see Figs. 5(b) and Figs. 5(h)]. It follows that Fermi arcs can be observed in polarization patterns.

D. The regime of the same mode numbers m: $X(m)$ and $Y(m)$

In the special case of almost degenerate modes with the same mode number m, for which $n_X \approx n_Y$, i.e., for $\overset{o}{\omega}_{X(m)} \approx \overset{o}{\omega}_{Y(m)}$ [see Figs. 3(e) and 3(f)], there exists a direct coupling quadratic in $\boldsymbol{k}$ between two bands through the matrix $\mathbf{B}_1$ [Eq. (32)]. In this case the effective Hamiltonian can be written in the same form as in Eq. (47):

$$\mathcal{H}' = \left(\omega_0 + i\Gamma_0 + \frac{\hbar k_x^2}{2m_x} + \frac{\hbar k_y^2}{2m_y}\right)\boldsymbol{\sigma}_0 - 2\beta k_x k_y \boldsymbol{\sigma}_x$$
$$+ \left(\Delta + i\delta\Gamma + \delta_x k_x^2 + \delta_y k_y^2\right)\boldsymbol{\sigma}_z - 2i\gamma k_x k_y \boldsymbol{\sigma}_y, \quad (49)$$

where m_x and m_y are effective masses of a photon in a cavity, the coefficients Δ, δ_x, δ_y, and γ are parameters that appeared as a result of the birefringence in the system, β is an effect of direct coupling between two orthogonal modes, and $\delta\Gamma$ corresponds to the difference between the values of ζ_X and ζ_Y, i.e., the difference in reflectivities of mirrors for two orthogonal polarizations. Using the formula for the modified Hamiltonian [Eq. (36)], we derived all parameters of Hamiltonian (49) and the results are presented as Eq. (C8) in Appendix C 3.

The coefficient γ is different from zero only if the energies of two modes are different, so that in the not fully degenerate situation we have an additional non-Hermitian element in the Hamiltonian matrix, related to the birefringence of the system. In contrast to the $X(m+2)$, $Y(m)$ case, the coefficient β
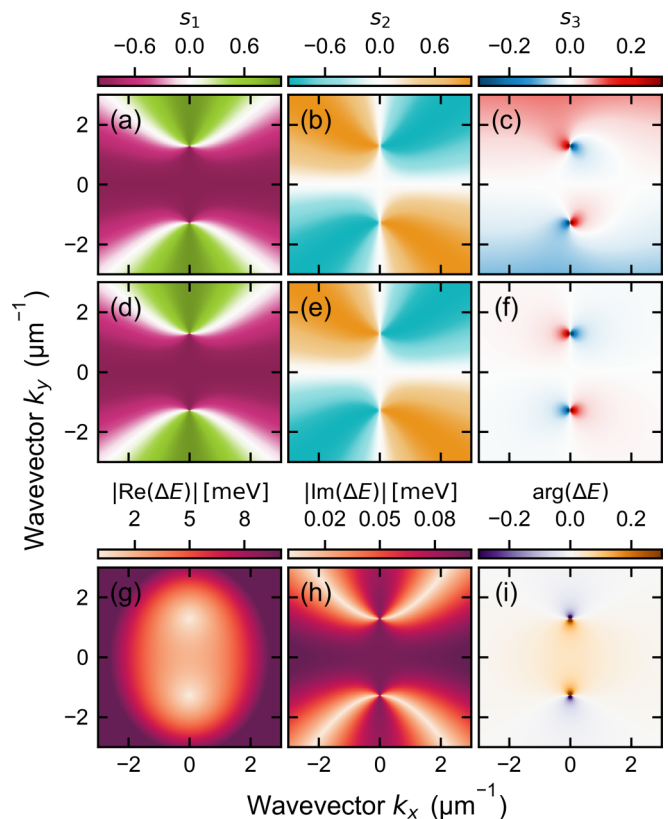

FIG. 6. The same mode number $X(m)$, $Y(m)$ regime. Stokes polarization parameters [(a) and (d)] s_1, [(b) and (e)] s_2, and [(c) and (f)] s_3 for upper energy branch in $\boldsymbol{k}$ space. The Stokes polarization parameters in (a)–(c) were calculated including an additional rotation of basis (see Appendix E) and in (d)–(f) they were calculated without taking into account additional rotation of basis. [(g)–(i)] The absolute values of real and imaginary parts and the phase of difference between two eigenvalues of Hamiltonian (49), $\Delta E = E_+ - E_-$.

is dominated by the direct coupling between horizontal and vertical modes through the matrix $\mathbf{B}_1$ [Eq. (32)].

Figure 6 presents the results obtained by diagonalization of two-mode Hamiltonian (49). Figures 6(a)–6(c) and 6(d)–6(f) present Stokes polarization parameters for the upper energy branch as a function of $\boldsymbol{k}$ calculated with the additional rotation of basis according to formulas presented in Appendix E and without it, respectively. Including these modifications turned out to be crucial as otherwise the Stokes polarization parameter s_3 would be large only close to the exceptional points and negligibly small for other $\boldsymbol{k}$ [see Figs. 6(c) and 6(f)].

The analytical formula for two-mode Hamiltonian (49) can be easily adopted to determine the expression for positions of topological points in $\boldsymbol{k}$ space. In this regime the degeneracy of real [Fig. 6(g)] and imaginary [Fig. 6(h)] parts of the energy occurs along four Fermi arcs connected by four exceptional points [see Fig. 6(i)] at which we observe degeneracy of both parts of the energies. The two-mode Hamiltonian (49) for this case has the same form as in the $X(m+2)$, $Y(m)$ regime [Eq. (47)], so the general solution for exceptional points is the same as in Eq. (48), but in this case $\Delta < 0$, $\delta'_x < 0$, $\delta'_y > 0$, and

$\beta' < \gamma' < 0$, where $x' = \mathrm{Re}(x)$, yield only four exceptional points with positions defined by the following equations:

$$k_{e,x} = \pm \sqrt{-\frac{\Delta + \sqrt{\Delta^2 - \frac{\delta\Gamma^2 \delta'_x \delta'_y}{(\beta')^2 - (\gamma')^2}}}{2\delta'_x}} \xrightarrow{\Delta \gg \delta\Gamma}$$

$$\pm \frac{1}{2}\sqrt{-\frac{\delta'_y}{((\beta')^2 - (\gamma')^2)\Delta}} \, \delta\Gamma, \tag{50a}$$

$$k_{e,y} = \pm \sqrt{\frac{-\Delta + \sqrt{\Delta^2 - \frac{\delta\Gamma^2 \delta'_x \delta'_y}{(\beta')^2 - (\gamma')^2}}}{2\delta'_y}} \xrightarrow{\Delta \gg \delta\Gamma}$$

$$\pm \sqrt{-\frac{\Delta}{\bar{\delta}_y}\left(1 - \frac{\delta'_x \delta'_y \delta\Gamma^2}{8\Delta^2((\beta')^2 - (\gamma')^2)}\right)}. \tag{50b}$$

The k_x component of exceptional points is very close to zero and mainly depends on the difference between lifetimes for two orthogonal polarizations ($\delta\Gamma$), but the k_y component of exceptional points can be smoothly changed by changing the detuning in system (Δ).

Again, the local maximum of s_2 Stokes polarization parameters occurs along the Fermi arcs for the imaginary part of the energy [see Figs. 6(b) and 6(h)], which proves that in such a regime the observation of such Fermi arcs can be performed by analyzing the polarization patterns. The abrupt change of s_1 polarization parameter is connected with the Fermi arcs for the real part of the energy [see Figs. 6(a) and 6(g)].

E. The comparison with other models

In Appendix G we present graphical comparison of results obtained with two-mode Hamiltonian (36), multimode Hamiltonian (32), and the numerical calculations using the Berreman-Schubert transfer matrix method [38,39]. The results of this third method are based on the transfer matrix approach obtained for δ mirrors introduced in detail in Appendix F. The $\mathbf{k} \cdot \mathbf{p}$ perturbation theory used for derivation of the two-mode Hamiltonian is a low-momentum approximation and provides satisfactory results for the in-plane momenta accessible in typical optical experiments [16,23,26,27,32,33,35,36,51]. A satisfactory convergence between the results presented in Appendix G and in this section is obtained provided that the modified basis set, as presented in Appendix E, is used for calculating the Stokes polarization parameters.

V. CONCLUSIONS

We have presented an effective theory of optical cavities based on the two-mode coupling approximation. It was demonstrated that taking into account the modifications of basic modes due to the coupling with other modes was essential for an accurate description of the positions of exceptional points corresponding to degeneracy of modes and light polarization pattern in their vicinity. The big advantage of this approach is that the resulting non-Hermitian 2×2 Hamiltonian matrix can be used to obtain quantitative results in analytical form. We have worked out an example in which the cavity mirrors are modeled by infinitely thin dielectric

layers. Our approach is, however, valid for any type of cavity mirrors, including multilayer distributed Bragg reflectors. Our model is exact up to quadratic order in the in-plane wave vector and all the effects, in particular those linear in $\mathbf{k}$, related to birefringence are taken into account without any further approximation. Accurate calculations using the Berreman method in the case of zero birefringence indicate almost invisible TE-TM splitting, which is in complete agreement with our approximate theory. On the other hand, adding even very small birefringence in the cavity medium results in large TE-TM splitting, mostly due to the term linear in $\mathbf{k}$. Even though the proposed scheme is limited to narrow incidence angles, our recent calculations (unpublished) show that the effective Hamiltonians can be applied to describe the experimental data also in the case of systems with patterned layers. The transmission of light through a birefringent microcavity with permeable mirrors was studied by using the Green's function approach based on Mittag-Leffler expansion of the resonant cavity states. Our method applies the $\mathbf{k} \cdot \mathbf{p}$ perturbation theory used in semiconductor physics, allowing us to describe the cavity modal dispersion and the modal electric field, which can be related to experimental studies of light polarization in cavities filled with the anisotropic (birefringent) medium in which the direction of the anisotropy axis can be smoothly tuned in a very broad range by applying external voltage.

We discussed three different scenarios described in terms of appropriate effective, non-Hermitian Hamiltonians. We verified our two-mode approximation by comparing it with more accurate methods, one of which included multimode analysis, and the other used the standard Berreman approach. It should be emphasized that our method allows for simplification and thus acceleration of calculations compared to the commonly used techniques based on the transfer matrix method. This observation becomes extremely important when solving problems where the dielectric tensor depends on position—like in optical lattices or other structures. Usually, in such cases, the finite-difference time-domain method, effective Hamiltonians on the lattice in real space, or Hamiltonians expanded in the Fourier basis are used. Unfortunately, both dimensions of the associated parameter space and the computation time greatly increase. In addition, our Hamiltonian allows us to analyze the properties of exceptional points which occur in non-Hermitian systems. The obtained analytical form and proper description of polarization opens new perspectives for investigating other topological properties of light in optical cavities, like characteristic polarization points of purely circular or linear polarization (so-called C points and L points), or elements of the quantum geometric tensor. This method will further be extended to strong light-matter-coupled systems such as the polariton laser and polariton condensate. Thanks to its simple structure, our model offers the possibility to control the topological properties of light by appropriately designing the components of the cavity structure affecting, for example, the anisotropy of the mirrors and the cavity material.

APPENDIX A: DERIVATION OF GREEN'S FUNCTION

Inserting the Green's function from Eq. (8) into Eq. (6) yields

$$
\left((\partial_z - \mathbf{A}^T)(\partial_z - \mathbf{A}) - \mathbf{B} + \frac{\omega^2}{c^2}\mathbf{B}_0\right)\frac{\mathbf{C}_r(z,z')}{\omega^2 - \omega_r^2}
$$
$$
+ \left((\partial_z - \mathbf{A}^T)(\partial_z - \mathbf{A}) - \mathbf{B} + \frac{\omega^2}{c^2}\mathbf{B}_0\right)\mathbf{M}_r(z,z')
$$
$$
= \left((\partial_z - \mathbf{A}^T)(\partial_z - \mathbf{A}) - \mathbf{B} + \frac{\omega_r^2}{c^2}\mathbf{B}_0\right)\frac{\mathbf{C}_r(z,z')}{\omega^2 - \omega_r^2}
$$
$$
+ \left((\partial_z - \mathbf{A}^T)(\partial_z - \mathbf{A}) - \mathbf{B} + \frac{\omega^2}{c^2}\mathbf{B}_0\right)\mathbf{M}_r(z,z')
$$
$$
+ \frac{1}{c^2}\mathbf{B}_0\mathbf{C}_r(z,z') = \mathbf{I}\delta(z-z'). \tag{A1}
$$

Comparing the singular and nonsingular parts of the left- and right-hand sides of Eq. (A1) gives the equations for $\mathbf{C}_r(z,z')$ and $\mathbf{M}_r(z,z')$:

$$
\left((\partial_z - \mathbf{A}^T)(\partial_z - \mathbf{A}) - \mathbf{B} + \frac{\omega_r^2}{c^2}\mathbf{B}_0\right)\mathbf{C}_r(z,z') = 0 \tag{A2a}
$$

and

$$
\left((\partial_z - \mathbf{A}^T)(\partial_z - \mathbf{A}) - \mathbf{B} + \frac{\omega^2}{c^2}\mathbf{B}_0\right)\mathbf{M}_r(z,z')
$$
$$
+ \frac{1}{c^2}\mathbf{B}_0\mathbf{C}_r(z,z') = \mathbf{I}\delta(z-z'). \tag{A2b}
$$

Applying the adjoint operator $\hat{\boldsymbol{\mathcal{L}}}^\dagger(z')$ to $\mathbf{G}^T(z,z')$ gives similarly

$$
\left((\partial_{z'} + \mathbf{A}^T)(\partial_{z'} + \mathbf{A}) - \mathbf{B}^T + \frac{\omega_r^2}{c^2}\mathbf{B}_0\right)\mathbf{C}_r^T(z,z') = 0 \tag{A3a}
$$

and

$$
\left((\partial_{z'} + \mathbf{A}^T)(\partial_{z'} + \mathbf{A}) - \mathbf{B}^T + \frac{\omega^2}{c^2}\mathbf{B}_0\right)\mathbf{M}_r^T(z,z')
$$
$$
+ \frac{1}{c^2}\mathbf{B}_0\mathbf{C}_r^T(z,z') = \mathbf{I}\delta(z-z'). \tag{A3b}
$$

The boundary conditions for $\mathbf{C}_r$ and $\mathbf{M}_r$ follow from Eq. (7):

$$
\partial_z\left(\frac{\mathbf{C}_r(z,z')}{\omega^2 - \omega_r^2} + \mathbf{M}_r(z,z')\right) = \pm ik_z\left(\frac{(\mathbf{C}_r(z,z'))}{\omega^2 - \omega_r^2} + \mathbf{M}_r(z,z')\right),
$$
$$
\tag{A4}
$$

where the upper sign refers to the points with $z > b$ and the lower sign corresponds to $z < a$. Taking into account that

$\omega^2 = (k_z^2 + k^2)c^2/n_a^2$ and similarly for the resonant frequency $\omega_r^2 = (k_{zr}^2 + k^2)c^2/n_a^2$, we obtain

$$
\partial_z\left(\frac{\mathbf{C}_r(z,z')}{\omega^2 - \omega_r^2} + \mathbf{M}_r(z,z')\right)
$$
$$
= \pm i\left(\frac{(k_z - k_{zr} + k_{zr})\mathbf{C}_r(z,z')n_a^2}{c^2(k_z - k_{zr})(k_z + k_{zr})} + k_z\mathbf{M}_r(z,z')\right)
$$
$$
= \pm i\left(\frac{\mathbf{C}_r(z,z')n_a^2}{c^2(k_z + k_{zr})} + k_{zr}\frac{\mathbf{C}_r(z,z')}{\omega^2 - \omega_r^2} + k_z\mathbf{M}_r(z,z')\right). \tag{A5}
$$

Comparing the regular and singular parts on both sides in the limit $k_z \to k_{zr}$ ($\omega \to \omega_r$) leads to the following boundary conditions for $\mathbf{C}_r$,

$$
\partial_z\mathbf{C}_r(z,z') = \pm ik_{zr}\mathbf{C}_r(z,z'), \tag{A6}
$$

and for $\mathbf{M}_r$,

$$
\partial_z\mathbf{M}_r(z,z') = \pm ik_{zr}\left(\mathbf{M}_r(z,z') + \frac{\mathbf{C}_r(z,z')n_a^2}{2c^2k_{zr}^2}\right), \tag{A7}
$$

which applies to the region outside of the cavity layers. Analogous boundary conditions apply to the derivatives with respect to z'. It follows then from Eq. (A2a) and Eq. (A3a) that

$$
\mathbf{C}_r(z,z') = \boldsymbol{u}_r(z)\boldsymbol{w}_r^T(z'), \tag{A8}
$$

where $\boldsymbol{u}_r(z)$ and $\boldsymbol{w}_r(z')$ are the resonant solutions of two coupled equations:

$$
\left((\partial_z - \mathbf{A}^T)(\partial_z - \mathbf{A}) - \mathbf{B} + \frac{\omega_r^2}{c^2}\mathbf{B}_0\right)\boldsymbol{u}_r(z) = 0, \tag{A9a}
$$

$$
\left((\partial_z + \mathbf{A}^T)(\partial_z + \mathbf{A}) - \mathbf{B}^T + \frac{\omega_r^2}{c^2}\mathbf{B}_0\right)\boldsymbol{w}_r(z) = 0, \tag{A9b}
$$

with outgoing wave boundary conditions

$$
\partial_z\boldsymbol{u}_r(z) = \pm ik_{zr}\boldsymbol{u}_r(z), \quad \partial_z\boldsymbol{w}_r(z) = \pm ik_{zr}\boldsymbol{w}_r(z). \tag{A10}
$$

The normalization condition for $\boldsymbol{u}_r$ and $\boldsymbol{w}_r$ is found by applying the generalized Green's formula and Eqs. (A2b) and (A8):

$$
\boldsymbol{w}_r^T(z)\left((\partial_z - \mathbf{A}^T)(\partial_z - \mathbf{A}) - \mathbf{B} + \frac{\omega_r^2}{c^2}\mathbf{B}_0\right)\mathbf{M}_r(z,z')
$$
$$
- \left[\mathbf{M}_r^T(z,z')\left((\partial_z + \mathbf{A}^T)(\partial_z + \mathbf{A}) - \mathbf{B}^T\right.\right.
$$
$$
\left.\left. + \frac{\omega_r^2}{c^2}\mathbf{B}_0\right)\boldsymbol{w}_r(z)\right]^T
$$
$$
= \partial_z\left(\boldsymbol{w}_r^T\partial_z\mathbf{M}_r - (\partial_z\boldsymbol{w}_r^T)\mathbf{M}_r - \boldsymbol{w}_r^T\mathbf{A}^T\mathbf{M}_r - \boldsymbol{w}_r^T\mathbf{A}\mathbf{M}_r\right)
$$
$$
= \boldsymbol{w}_r^T(z)\left(\delta(z-z') - \frac{1}{c^2}\mathbf{B}_0\boldsymbol{u}_r(z)\boldsymbol{w}_r^T(z')\right). \tag{A11}
$$

Integrating both sides with respect to z from a to b and taking into account that $\mathbf{A} \neq 0$ only in the birefringent layer yields, for $a < z' < b$,

$$
\left(\boldsymbol{w}_r^T(z)\partial_z\mathbf{M}_r(z,z') - (\partial_z\boldsymbol{w}_r^T)\mathbf{M}_r(z,z')\right)\big|_{z=a}^{z=b}
$$
$$
= \left(1 - \frac{1}{c^2}\int_a^b \boldsymbol{w}_r^T(z)\mathbf{B}_0(z)\boldsymbol{u}_r(z)dz\right)\boldsymbol{w}_r^T(z'). \tag{A12}
$$

Taking into account the boundary conditions for $\mathbf{M}_r(z, z')$ [Eq. (A7)] and for $\boldsymbol{w}_r$ [Eq. (A10)] we arrive at

$$\frac{in_a^2}{2c^2 k_{zr}}\left(\boldsymbol{w}_r^T(b)\boldsymbol{u}_r(b) + \boldsymbol{w}_r^T(a)\boldsymbol{u}_r(a)\right)\boldsymbol{w}_r^T(z')$$

$$= \left(1 - \frac{1}{c^2}\int_a^b \boldsymbol{w}_r^T(z)\mathbf{B}_0(z)\boldsymbol{u}_r(z)dz\right)\boldsymbol{w}_r^T(z'), \quad \text{(A13)}$$

so the normalization condition for $\boldsymbol{u}_r$ and $\boldsymbol{w}_r$ has the form

$$\frac{1}{c^2}\int_a^b \boldsymbol{w}_r^T(z)\mathbf{B}_0(z)\boldsymbol{u}_r(z)dz$$

$$+ \frac{in_a^2}{2c^2 k_{zr}}\left(\boldsymbol{w}_r^T(b)\boldsymbol{u}_r(b) + \boldsymbol{w}_r^T(a)\boldsymbol{u}_r(a)\right) = 1. \quad \text{(A14)}$$

APPENDIX B: DERIVATION OF THE EIGENEQUATION FOR RESONANT MODES

Equation (16) leads to the following representation of Green's functions $\mathbf{G}$ and $\mathbf{G}_0$ as sums over simple poles associated with the resonant states:

$$\mathbf{G}(z, z'; \omega, \boldsymbol{k}) = \sideset{}{'}\sum_m \frac{\boldsymbol{u}_m(z)\boldsymbol{w}_m^T(z')}{2\omega_m(\boldsymbol{k})(\omega - \omega_m(\boldsymbol{k}))}, \quad \text{(B1)}$$

and since $\overset{o}{\boldsymbol{w}}{}_m^T(z) = \overset{o}{\boldsymbol{u}}{}_m^T(z)$ [Eqs. (A9) and (19)],

$$\mathbf{G}_0(z, z'; \omega, \boldsymbol{k}) = \sideset{}{'}\sum_m \frac{\overset{o}{\boldsymbol{u}}_m(z)\overset{o}{\boldsymbol{u}}{}_m^T(z')}{2\overset{o}{\omega}_m(\boldsymbol{k})\left(\omega - \overset{o}{\omega}_m(\boldsymbol{k})\right)}, \quad \text{(B2)}$$

where the summation is limited to the poles in the lower half of the complex ω plane including the pole at zero if it exists [48]. The Dyson equation for $\mathbf{G}$,

$$\mathbf{G}(z, z') = \mathbf{G}_0(z, z') - \int_a^b \mathbf{G}_0(z, z'')\hat{\boldsymbol{\mathcal{L}}}'(z'')\mathbf{G}(z'', z') \, dz'', \quad \text{(B3)}$$

leads to

$$\sideset{}{'}\sum_n \frac{\boldsymbol{u}_n(z)\boldsymbol{w}_n^T(z')}{2\omega_n(\boldsymbol{k})(\omega - \omega_n(\boldsymbol{k}))}$$

$$= \sideset{}{'}\sum_m \frac{\overset{o}{\boldsymbol{u}}_m(z)\overset{o}{\boldsymbol{u}}{}_m^T(z')}{2\overset{o}{\omega}_m(\boldsymbol{k})(\omega - \overset{o}{\omega}_m(\boldsymbol{k}))}$$

$$- \int_a^b \sideset{}{'}\sum_{mn} \frac{\overset{o}{\boldsymbol{u}}_m(z)\overset{o}{\boldsymbol{u}}{}_m^T(z'')\hat{\boldsymbol{\mathcal{L}}}'(z'')\boldsymbol{u}_n(z'')\boldsymbol{w}_n^T(z')}{2\overset{o}{\omega}_m(\boldsymbol{k})(\omega - \overset{o}{\omega}_m(\boldsymbol{k}))2\omega_n(\boldsymbol{k})(\omega - \omega_n(\boldsymbol{k}))}dz''. \quad \text{(B4)}$$

Comparing residua at $\omega_n(\boldsymbol{k})$ on both sides gives

$$\boldsymbol{u}_n(z) = -\int_a^b \sideset{}{'}\sum_m \frac{\overset{o}{\boldsymbol{u}}_m(z)\overset{o}{\boldsymbol{u}}{}_m^T(z'')\hat{\boldsymbol{\mathcal{L}}}'(z'')\boldsymbol{u}_n(z'')}{2\overset{o}{\omega}_m(\boldsymbol{k})(\omega_n(\boldsymbol{k}) - \overset{o}{\omega}_m(\boldsymbol{k}))}dz''. \quad \text{(B5)}$$

Inserting Eq. (21) leads to

$$\sum_m \frac{a_{mn}}{\sqrt{\overset{o}{\omega}_m(\boldsymbol{k})}}\overset{o}{\boldsymbol{u}}_m$$

$$= -\sum_{mp} \frac{\overset{o}{\boldsymbol{u}}_m(z)(\hat{\boldsymbol{\mathcal{L}}}')_{mp}a_{pn}}{2\sqrt{\overset{o}{\omega}_p(\boldsymbol{k})}\overset{o}{\omega}_m(\boldsymbol{k})(\omega_n(\boldsymbol{k}) - \overset{o}{\omega}_m(\boldsymbol{k}))}, \quad \text{(B6)}$$

where

$$(\hat{\boldsymbol{\mathcal{L}}}')_{mp} = \int_a^b \overset{o}{\boldsymbol{u}}{}_m^T(z'')\hat{\boldsymbol{\mathcal{L}}}'(z'')\overset{o}{\boldsymbol{u}}_p(z'')dz''. \quad \text{(B7)}$$

Comparing coefficients at the $\overset{o}{\boldsymbol{u}}_m$ we obtain the equations for the coefficient a_{mn},

$$a_{mn} = -\sum_p \frac{(\hat{\boldsymbol{\mathcal{L}}}')_{mp}a_{pn}}{2\sqrt{\overset{o}{\omega}_m(\boldsymbol{k})\overset{o}{\omega}_p(\boldsymbol{k})}(\omega_n(\boldsymbol{k}) - \overset{o}{\omega}_m(\boldsymbol{k}))}, \quad \text{(B8)}$$

which can be written in the form of an eigenequation for the nth column of the a_{mn} matrix:

$$\omega_n(\boldsymbol{k})a_{mn} = \sum_p \left(\overset{o}{\omega}_m(\boldsymbol{k})\delta_{mp} - \frac{(\hat{\boldsymbol{\mathcal{L}}}')_{mp}}{2\sqrt{\overset{o}{\omega}_m(\boldsymbol{k})\overset{o}{\omega}_p(\boldsymbol{k})}}\right)a_{pn}. \quad \text{(B9)}$$

APPENDIX C: PARAMETERS OF TWO-MODE HAMILTONIANS

In this Appendix we give the expressions for the parameters of the two-mode Hamiltonians, based on the formula presented in Eq. (36). We introduce auxiliary parameters:

$$\eta^{m',m} = \sqrt{\frac{\overset{o}{\omega}_{X(m')}}{\overset{o}{\omega}_{Y(m)}}}, \quad \text{(C1a)}$$

$$m_0^{m',m} = \frac{\hbar\sqrt{\overset{o}{\omega}_{X(m')}\overset{o}{\omega}_{Y(m)}}}{c^2}, \quad \text{(C1b)}$$

$$a_x^{m',m} = \frac{1}{\tilde{\varepsilon}_{xx}}\left(\frac{\varepsilon_{xx}}{\varepsilon_{zz}} + 4\frac{\varepsilon_{xz}^2}{\varepsilon_{zz}}f_{X(m'),X(m')}(X)\right), \quad \text{(C1c)}$$

$$b_x^{m',m} = \frac{1}{\varepsilon_{yy}}, \quad \text{(C1d)}$$

$$a_y^{m',m} = \frac{1}{\tilde{\varepsilon}_{xx}}\left(1 + \frac{\varepsilon_{xz}^2}{\varepsilon_{zz}^2}(1 + f_{X(m'),X(m')}(Y))\right), \quad \text{(C1e)}$$

$$b_y^{m,m'} = \frac{1}{\varepsilon_{yy}}\left(\frac{\varepsilon_{yy}}{\varepsilon_{zz}} + \frac{\varepsilon_{xz}^2}{\varepsilon_{zz}^2}f_{Y(m),Y(m)}\right), \quad \text{(C1f)}$$

$$a^{m',m} = \frac{\tilde{\varepsilon}_{xx} - \varepsilon_{zz}}{2\varepsilon_{zz}}P_{X(m'),Y(m)} + \frac{\varepsilon_{xz}^2}{\varepsilon_{zz}^2}f_{X(m'),Y(m)}(X), \quad \text{(C1g)}$$

$$b^{m',m} = \frac{\varepsilon_{yy} - \varepsilon_{zz}}{2\varepsilon_{zz}}P_{X(m'),Y(m)} + \frac{\varepsilon_{xz}^2}{\varepsilon_{zz}^2}f_{X(m'),Y(m)}(X), \quad \text{(C1h)}$$

where $f_{sm,s'm'}(s'')$ according to Eq. (36) represents the correction from interaction with states which do not belong to the

set $\{\boldsymbol{E}_{X(m')}(z), \boldsymbol{E}_{Y(m)}(z)\}$ and is equal to

$$f_{sm,s'm'}(s'') = -\sum_{n''}{}' \frac{c^2}{4\overset{o}{\omega}_{s''m''}n^2_{s''}} Q_{sm,s''m''}Q_{s''m'',s'm'}$$
$$\times \left(\frac{1}{(\overset{o}{\omega}_{sm} - \overset{o}{\omega}_{s''m''})} + \frac{1}{(\overset{o}{\omega}_{s'm'} - \overset{o}{\omega}_{s''m''})}\right), \tag{C2}$$

where the summation for the polarization s'' includes all states outside the set $\{\boldsymbol{E}_{X(m')}(z), \boldsymbol{E}_{Y(m)}(z)\}$. It is worth noting that the overall integral $Q_{sm,s''m''}$ vanishes if m and m'' are of the same parity.

1. The regime of modes with opposite parity, $X(m+1)$ and $Y(m)$: Rashba-Dresselhaus spin-orbit coupling

$$\omega_0 = \mathrm{Re}[(\overset{o}{\omega}_{X(m+1)} + \overset{o}{\omega}_{Y(m)})/2], \tag{C3a}$$

$$\Gamma_0 = \mathrm{Im}[(\overset{o}{\omega}_{X(m+1)} + \overset{o}{\omega}_{Y(m)})/2], \tag{C3b}$$

$$\Delta = \mathrm{Re}[(\overset{o}{\omega}_{X(m+1)} - \overset{o}{\omega}_{Y(m)})/2], \tag{C3c}$$

$$\delta\Gamma = \mathrm{Im}[(\overset{o}{\omega}_{X(m+1)} - \overset{o}{\omega}_{Y(m)})/2], \tag{C3d}$$

$$\frac{1}{m_x} = \frac{1}{2m_0^{m+1,m}}\left(\frac{a_x^{m+1,m}}{\eta^{m+1,m}} + b_x^{m+1,m}\eta^{m+1,m}\right), \tag{C4a}$$

$$\frac{1}{m_y} = \frac{1}{2m_0^{m+1,m}}\left(\frac{a_y^{m+1,m}}{\eta^{m+1,m}} + b_y^{m+1,m}\eta^{m+1,m}\right), \tag{C4b}$$

$$\delta_x = \frac{\hbar}{4m_0^{m+1,m}}\left(\frac{a_x^{m+1,m}}{\eta^{m+1,m}} - b_x^{m+1,m}\eta^{m+1,m}\right), \tag{C4c}$$

$$\delta_y = \frac{\hbar}{4m_0^{m+1,m}}\left(\frac{a_y^{m+1,m}}{\eta^{m+1,m}} - b_y^{m+1,m}\eta^{m+1,m}\right), \tag{C4d}$$

$$\alpha = -\frac{\hbar}{4m_0}\frac{\varepsilon_{xz}}{n_X n_Y \varepsilon_{zz}}Q_{X(m+1),Y(m)}. \tag{C4e}$$

2. The regime of modes of the same parity: $X(m+2)$ and $Y(m)$

$$\omega_0 = \mathrm{Re}[(\overset{o}{\omega}_{X(m+2)} + \overset{o}{\omega}_{Y(m)})/2], \tag{C5a}$$

$$\Gamma_0 = \mathrm{Im}[(\overset{o}{\omega}_{X(m+2)} + \overset{o}{\omega}_{Y(m)})/2], \tag{C5b}$$

$$\Delta = \mathrm{Re}[(\overset{o}{\omega}_{X(m+2)} - \overset{o}{\omega}_{Y(m)})/2], \tag{C5c}$$

$$\delta\Gamma = \mathrm{Im}[(\overset{o}{\omega}_{X(m+2)} - \overset{o}{\omega}_{Y(m)})/2], \tag{C5d}$$

$$\frac{1}{m_x} = \frac{1}{2m_0^{m+2,m}}\left(\frac{a_x^{m+2,m}}{\eta^{m+2,m}} + b_x^{m+2,m}\eta^{m+2,m}\right), \tag{C6a}$$

$$\frac{1}{m_y} = \frac{1}{2m_0^{m+2,m}}\left(\frac{a_y^{m+2,m}}{\eta^{m+2,m}} + b_y^{m+2,m}\eta^{m+2,m}\right), \tag{C6b}$$

$$\delta_x = \frac{\hbar}{4m_0^{m+2,m}}\left(\frac{a_x^{m+2,m}}{\eta^{m+2,m}} - b_x^{m+2,m}\eta^{m+2,m}\right), \tag{C6c}$$

$$\delta_y = \frac{\hbar}{4m_0^{m+2,m}}\left(\frac{a_y^{m+2,m}}{\eta^{m+2,m}} - b_y^{m+2,m}\eta^{m+2,m}\right), \tag{C6d}$$

$$\beta = -\frac{\hbar}{4m_0^{m+2,m}n_X n_Y}(a^{m+2,m} + b^{m+2,m}), \tag{C6e}$$

$$\gamma = \frac{\hbar}{4m_0^{m+2,m}n_X n_Y}(a^{m+2,m} - b^{m+2,m}). \tag{C6f}$$

3. The regime of the same mode numbers m: $X(m)$ and $Y(m)$

$$\omega_0 = \mathrm{Re}[(\overset{o}{\omega}_{X(m)} + \overset{o}{\omega}_{Y(m)})/2], \tag{C7a}$$

$$\Gamma_0 = \mathrm{Im}[(\overset{o}{\omega}_{X(m)} + \overset{o}{\omega}_{Y(m)})/2], \tag{C7b}$$

$$\Delta = \mathrm{Re}[(\overset{o}{\omega}_{X(m)} - \overset{o}{\omega}_{Y(m)})/2], \tag{C7c}$$

$$\delta\Gamma = \mathrm{Im}[(\overset{o}{\omega}_{X(m)} - \overset{o}{\omega}_{Y(m)})/2], \tag{C7d}$$

$$\frac{1}{m_x} = \frac{1}{2m_0^{m,m}}\left(\frac{a_x^{m,m}}{\eta^{m,m}} + b_x^{m,m}\eta^{m,m}\right), \tag{C8a}$$

$$\frac{1}{m_y} = \frac{1}{2m_0^{m,m}}\left(\frac{a_y^{m,m}}{\eta^{m,m}} + b_y^{m,m}\eta^{m,m}\right), \tag{C8b}$$

$$\delta_x = \frac{\hbar}{4m_0^{m,m}}\left(\frac{a_x^{m,m}}{\eta^{m,m}} - b_x^{m,m}\eta^{m,m}\right), \tag{C8c}$$

$$\delta_y = \frac{\hbar}{4m_0^{m,m}}\left(\frac{a_y^{m,m}}{\eta^{m,m}} - b_y^{m,m}\eta^{m,m}\right), \tag{C8d}$$

$$\beta = -\frac{\hbar}{4m_0^{m,m}n_X n_Y}(a^{m,m} + b^{m,m}), \tag{C8e}$$

$$\gamma = \frac{\hbar}{4m_0^{m,m}n_X n_Y}(a^{m,m} - b^{m,m}). \tag{C8f}$$

APPENDIX D: MAXWELL'S EQUATION FOR BIREFRINGENT SYSTEM

Similarly to Berreman's consideration, we assumed that the three-dimensional vectors of electric and magnetic fields could be written as

$$\vec{E}(x, y, z) = \vec{E}_{\boldsymbol{k}}(z)e^{i(k_0\boldsymbol{\kappa}\cdot\boldsymbol{r}-\omega t)}, \tag{D1a}$$

$$\vec{H}(x, y, z) = \vec{H}_{\boldsymbol{k}}(z)e^{i(k_0\boldsymbol{\kappa}\cdot\boldsymbol{r}-\omega t)}, \tag{D1b}$$

where $\boldsymbol{k}$ and $\boldsymbol{r}$ are two-dimensional wave and position vectors in the x-y plane, respectively, and $\boldsymbol{\kappa} = \boldsymbol{k}/k_0$, where $k_0 = \omega/c$. We begin with the Maxwell equations:

$$\vec{\nabla} \times \vec{E} = -\mu_0 \frac{\partial \vec{H}}{\partial t} \quad \text{and} \quad \vec{\nabla} \times \vec{H} = \varepsilon_0 \hat{\varepsilon} \frac{\partial \vec{E}}{\partial t}, \tag{D2}$$

where $\hat{\varepsilon}$ is a 3×3 matrix for the birefringent system, and μ_0 and ε_0 denote vacuum magnetic permeability and vacuum permittivity, respectively. Eliminating the z component of the electric and magnetic fields led to the following relationship:

$$\partial_z \begin{bmatrix} \boldsymbol{E} \\ \boldsymbol{H} \end{bmatrix} = \begin{bmatrix} \mathbf{S}_{11} & \mathbf{S}_{12} \\ \mathbf{S}_{21} & \mathbf{S}_{22} \end{bmatrix} \begin{bmatrix} \boldsymbol{E} \\ \boldsymbol{H} \end{bmatrix}, \tag{D3}$$

where $\boldsymbol{E}$ and $\boldsymbol{H}$ denote two-dimensional vectors of electric and magnetic fields in the x-y plane, respectively, and the

matrices $\mathbf{S}_{ij}$ are given by

$$\mathbf{S}_{11} = \frac{ik_0}{\varepsilon_{zz}}\begin{bmatrix} -\kappa_x\varepsilon_{zx} & -\kappa_x\varepsilon_{zy} \\ -\kappa_y\varepsilon_{zx} & -\kappa_y\varepsilon_{zy} \end{bmatrix}, \tag{D4a}$$

$$\mathbf{S}_{12} = \frac{ik_0\eta_0}{\varepsilon_{zz}}\begin{bmatrix} \kappa_x\kappa_y & \varepsilon_{zz}-\kappa_x^2 \\ \kappa_y^2-\varepsilon_{zz} & -\kappa_x\kappa_y \end{bmatrix}, \tag{D4b}$$

$$\mathbf{S}_{21} = \frac{ik_0}{\eta_0}\begin{bmatrix} -\tilde{\varepsilon}_{yx}-\kappa_x\kappa_y & -\tilde{\varepsilon}_{yy}+\kappa_x^2 \\ \tilde{\varepsilon}_{xx}-\kappa_y^2 & \tilde{\varepsilon}_{xy}+\kappa_x\kappa_y \end{bmatrix}, \tag{D4c}$$

$$\mathbf{S}_{22} = \frac{ik_0}{\varepsilon_{zz}}\begin{bmatrix} -\kappa_y\varepsilon_{yz} & \kappa_x\varepsilon_{yz} \\ \kappa_y\varepsilon_{xz} & -\kappa_x\varepsilon_{xz} \end{bmatrix}. \tag{D4d}$$

Here $\eta_0 = \sqrt{\mu_0/\varepsilon_0}$ and $\tilde{\varepsilon}_{ij} = \varepsilon_{ij} - \varepsilon_{iz}\varepsilon_{zj}/\varepsilon_{zz}$. Equation (D3) can be rewritten as

$$\boldsymbol{H} = \mathbf{S}_{12}^{-1}(\partial_z - \mathbf{S}_{11})\boldsymbol{E}, \tag{D5a}$$

$$\mathbf{S}_{21}\boldsymbol{E} = (\partial_z - \mathbf{S}_{22})\boldsymbol{H}. \tag{D5b}$$

Eliminating the magnetic field yields the exact equation for the electric field, $\hat{\mathcal{L}}_f\boldsymbol{E} = \boldsymbol{0}$, where the $\hat{\mathcal{L}}_f$ operator is given by

$$\hat{\mathcal{L}}_f = (\partial_z - \tilde{\mathbf{A}})(\partial_z - \tilde{\mathbf{B}}) - \tilde{\mathbf{C}} \tag{D6}$$

and

$$\tilde{\mathbf{A}} = \mathbf{S}_{12}\mathbf{S}_{22}\mathbf{S}_{12}^{-1} - \mathbf{S}_{12}(\partial_z\mathbf{S}_{12}^{-1}), \tag{D7a}$$

$$\tilde{\mathbf{B}} = \mathbf{S}_{11}, \tag{D7b}$$

$$\tilde{\mathbf{C}} = \mathbf{S}_{12}\mathbf{S}_{21}. \tag{D7c}$$

Note that the second term in Eq. (D7a) is different from zero only at the interfaces and it is smaller by a factor of at least k_0 from the leading terms in this expression and it will be neglected in the following. We can apply the Taylor series expansion in powers of κ in order to generate successive approximations to $\hat{\mathcal{L}}_f$:

$$\tilde{\mathbf{A}}^{(i)} = \sum_{j=0}^{i}\frac{\kappa_x^{i-j}\kappa_y^j}{j!(i-j)!}\frac{\partial^{i-j}}{\partial\kappa_x^{i-j}}\frac{\partial^j}{\partial\kappa_y^j}\tilde{\mathbf{A}}\bigg|_{\kappa_x=\kappa_y=0}, \tag{D8a}$$

$$\tilde{\mathbf{B}}^{(i)} = \sum_{j=0}^{i}\frac{\kappa_x^{i-j}\kappa_y^j}{j!(i-j)!}\frac{\partial^{i-j}}{\partial\kappa_x^{i-j}}\frac{\partial^j}{\partial\kappa_y^j}\tilde{\mathbf{B}}\bigg|_{\kappa_x=\kappa_y=0}, \tag{D8b}$$

$$\tilde{\mathbf{C}}^{(i)} = \sum_{j=0}^{i}\frac{\kappa_x^{i-j}\kappa_y^j}{j!(i-j)!}\frac{\partial^{i-j}}{\partial\kappa_x^{i-j}}\frac{\partial^j}{\partial\kappa_y^j}\tilde{\mathbf{C}}\bigg|_{\kappa_x=\kappa_y=0}. \tag{D8c}$$

Taking only the terms up to second order and comparing Eq. (4) with Eq. (D6), we obtained expressions for the matrices $\mathbf{A}$, $\mathbf{B}_0$, and $\mathbf{B}$:

$$\mathbf{A} = \tilde{\mathbf{B}}^{(1)} = (\tilde{\mathbf{A}}^{(1)})^T, \tag{D9a}$$

$$\mathbf{B}_0 = -\frac{1}{k_0^2}\tilde{\mathbf{C}}^{(0)}, \tag{D9b}$$

$$\mathbf{B} = \tilde{\mathbf{C}}^{(2)}. \tag{D9c}$$

In order to estimate the role of the neglected term in Eq. (D7a) we consider the case of an isotropic medium inside the cavity. The $\hat{\mathcal{L}}_f$ operator becomes then

$$\hat{\mathcal{L}}_{iso} = (\partial_z + \tilde{\mathbf{D}})\partial_z - \tilde{\mathbf{C}} \tag{D10}$$

since $\mathbf{S}_{11} = \mathbf{S}_{22} = \mathbf{0}$. Now we have

$$\tilde{\mathbf{C}} = k_0^2[\kappa_x^2 + \kappa_y^2 - \varepsilon(z)]\boldsymbol{\sigma}_0, \tag{D11a}$$

and

$$\tilde{\mathbf{D}} = \mathbf{S}_{12}(\partial_z\mathbf{S}_{12}^{-1})$$

$$= \frac{\varepsilon'(z)}{\varepsilon(z)[\kappa_x^2 + \kappa_y^2 - \varepsilon(z)]}\begin{bmatrix} \kappa_x^2 & \kappa_x\kappa_y \\ \kappa_x\kappa_y & \kappa_y^2 \end{bmatrix}, \tag{D11b}$$

where $\varepsilon(z)$ describes the dependence of relative permittivity on z. The matrix $\tilde{\mathbf{D}}$ can be diagonalized with eigenvalues,

$$\lambda_+ = 0, \quad \lambda_- = \frac{\varepsilon'(z)(\kappa_x^2 + \kappa_y^2)}{\varepsilon(z)[\kappa_x^2 + \kappa_y^2 - \varepsilon(z)]}, \tag{D12a}$$

and eigenvectors,

$$\boldsymbol{v}_+ = \begin{bmatrix} \kappa_y \\ -\kappa_x \end{bmatrix}, \quad \boldsymbol{v}_- = \begin{bmatrix} \kappa_x \\ \kappa_y \end{bmatrix}. \tag{D12b}$$

The electric field polarized along the $\boldsymbol{v}_+$ vector is continuous and smooth, because the corresponding eigenvalue $\lambda_+ = 0$. On the other hand, the derivative of the electric field for the second polarization, $\boldsymbol{v}_-$, has a finite discontinuity at the interfaces depending on $\varepsilon'(z)$ and the value of κ_x and κ_y. We thus conclude that the neglected term represented by $\tilde{\mathbf{D}}$ is responsible for the additional, angle-dependent TE-TM splitting in the cavities consisting of isotropic layers. This term is of the order $k_0^{-2}(k_x^2 + k_y^2)(1/\varepsilon(z))'$ so it is much smaller than the leading terms in our effective Hamiltonians. Clearly, the TE-TM splitting caused by the mirrors is much smaller than the splitting due to the birefringent medium inside the cavity, so in the first approximation it can be neglected (see Fig. 7).

APPENDIX E: POLARIZATION OF LIGHT IN TWO-MODE APPROXIMATION

The expansion of the modal electric field $\boldsymbol{E}$ in the perturbed basis is given by

$$\boldsymbol{E}(z, \boldsymbol{k}) = \sum_{sm}'\frac{a'_{sm}(\boldsymbol{k})}{\sqrt{\mathring{\omega}_{sm}}}\boldsymbol{E}'_{sm}(z, \boldsymbol{k}), \tag{E1}$$

where the sum over m extends over the subset of states of interest. Note that the perturbed basis functions $\boldsymbol{E}'_{sm}(z, \boldsymbol{k})$, in contrast to the unperturbed functions, depend on $\boldsymbol{k}$. We define the general formula for the polarization matrix in unperturbed and perturbed basis states:

$$(\hat{P}_i(z))_{sm,s'm'} = (\boldsymbol{E}_{sm}(z))^\dagger\boldsymbol{\sigma}_i\boldsymbol{E}_{s'm'}(z), \tag{E2a}$$

$$(\hat{P}'_i(z))_{sm,s'm'} = (\boldsymbol{E}'_{sm}(z))^\dagger\boldsymbol{\sigma}_i\boldsymbol{E}'_{s'm'}(z). \tag{E2b}$$

Applying Eq. (37), we obtain the following expression for the polarization matrices in the $z = 0$ plane:

$$(\hat{P}'_i(0))_{sm,s'm'} = \sum_{s''m''}\sum_{s'''m'''}(e^{\hat{R}^*})_{s''m'',sm}(\hat{P}_i(0))_{s''m'',s'''m'''}$$

$$\times (e^{\hat{R}})_{s'''m''',s'm'}, \tag{E3}$$

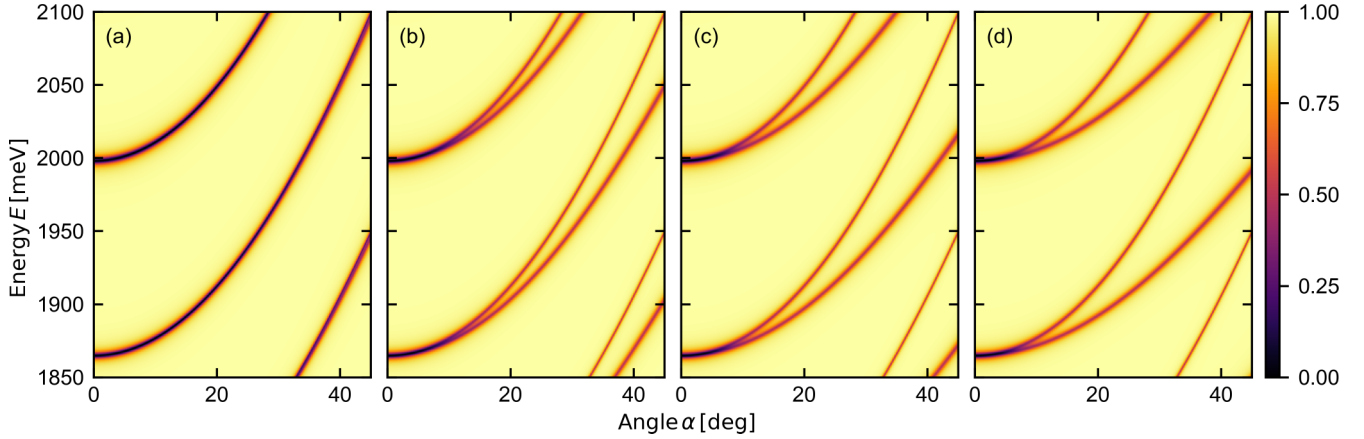where the sum is over all states. Up to the linear order of perturbation theory the components of the polarization

FIG. 7. Reflectance spectra for cavity with two δ mirrors filled by a medium characterized by $\hat{\varepsilon} = \mathrm{diag}(n_o^2, n_o^2, \gamma^2 n_o^2)$, where $\gamma \in \{1.0, 1.1, 1.2, 1.3\}$ for (a), (b), (c), and (d), respectively.

matrix and the Stokes polarization parameter are equal to

$$(\hat{P}'_i(0))_{sm,s'm'} = (\hat{P}_i)_{sm,s'm'} + \sum_{s''m''} R^*_{s''m'',sm}(\hat{P}_i(0))_{s''m'',s'm'} + (\hat{P}_i(0))_{sm,s''m''}R_{s''m'',s'm'}, \tag{E4}$$

$$s_i(0, \boldsymbol{k}) = \frac{1}{S_0} {\sum_{sm}}' {\sum_{s'm'}}' (a'_{sm}(\boldsymbol{k}))^* a'_{s'm'}(\boldsymbol{k}) \left((\hat{P}_i(0))_{sm,s'm'} + \sum_{s''m''} R^*_{s''m'',sm}(\hat{P}_i(0))_{s''m'',s'm'} + (\hat{P}_i(0))_{sm,s''m''}R_{s''m'',s'm'} \right), \tag{E5}$$

where

$$S_0 = {\sum_{sm}}' {\sum_{s'm'}}' \left(a'_{sm}(\boldsymbol{k}) \right)^* a'_{s'm'}(\boldsymbol{k}) \left((\hat{P}_0(0))_{sm,s'm'} + \sum_{s''m''} R^*_{s''m'',sm}(\hat{P}_0(0))_{s''m'',s'm'} + (\hat{P}_0(0))_{sm,s''m''}R_{s''m'',s'm'} \right). \tag{E6}$$

As it turns out the corrections to the polarization matrix introduced by the coupling to the modes which are not directly included in the two-mode model are crucial for proper description of the Stokes polarization parameters.

APPENDIX F: PROPAGATION OF LIGHT THROUGH THE CAVITY WITH δ MIRRORS

1. Transfer matrix for δ mirror

In order to verify the results obtained using the effective two-mode Hamiltonian (36) and the multimode Hamiltonian, Eq. (32), in the case of the model δ-like mirror profiles, we performed numerical calculations using the Berreman-Schubert transfer matrix method [38,39].

We assume that the thin mirror layer of width l is parallel to the x-y plane and is characterized by the isotropic dielectric constant $\varepsilon_r = -2\zeta/k_0^2 l$, where the mirror parameter ζ determines its strength and in general is polarization dependent. For a dielectric layer $\zeta < 0$ and for a metallic layer $\zeta > 0$. In the case of a perfect mirror, we have $\zeta = \pm\infty$. Assuming $\mu_r = 1$ the corresponding refractive index is $n = \sqrt{-2\zeta/k_0^2 l}$. The two-dimensional vectors of the electric and magnetic fields in this layer are given by

$$\boldsymbol{E}(\kappa, z) = \boldsymbol{A}(\kappa)e^{ik_0 nz} + \boldsymbol{B}(\kappa)e^{-ik_0 nz}, \tag{F1a}$$

$$\boldsymbol{H}(\kappa, z) = \mathbf{S}_{12}^{-1} \partial_z \boldsymbol{E}(\kappa, z), \tag{F1b}$$

where $\boldsymbol{A}(\kappa)$ and $\boldsymbol{B}(\kappa)$ denote the amplitudes of the electric field plane waves, and $\mathbf{S}_{12}$ is defined in Eq. (D3) with $\varepsilon_{zz} = \varepsilon_r$. After eliminating these amplitudes, we obtained the following matching conditions for the electric and magnetic fields on both sides of the layer:

$$\begin{bmatrix} \boldsymbol{E}(l) \\ \boldsymbol{H}(l) \end{bmatrix} = \begin{bmatrix} \cos(\alpha_n)\boldsymbol{\sigma}_0 & \frac{l}{\alpha_n}\sin(\alpha_n)\mathbf{S}_{12} \\ -\frac{\alpha_n}{l}\sin(\alpha_n)\mathbf{S}_{12}^{-1} & \cos(\alpha_n)\boldsymbol{\sigma}_0 \end{bmatrix} \begin{bmatrix} \boldsymbol{E}(0) \\ \boldsymbol{H}(0) \end{bmatrix}, \tag{F2}$$

where $\alpha_n = k_0 nl$. In the limit of an infinitely thin layer ($l \to 0$),

$$\begin{bmatrix} \boldsymbol{E}_{0^+} \\ \boldsymbol{H}_{0^+} \end{bmatrix} = \begin{bmatrix} \boldsymbol{\sigma}_0 & \mathbf{0} \\ -\frac{2\zeta}{k_0\eta_0}\boldsymbol{\sigma}_y & \boldsymbol{\sigma}_0 \end{bmatrix} \begin{bmatrix} \boldsymbol{E}_{0^-} \\ \boldsymbol{H}_{0^-} \end{bmatrix}. \tag{F3}$$

Consequently, the electric field is continuous across the thin mirror layer while the magnetic field suffers a discontinuity. Both the electric and magnetic fields are obviously continuous at the interfaces as they should be. Assuming an isotropic ($\varepsilon_{zz} = n_a^2$) medium on the left side of the layer (outside the cavity marked with a subscript $-$), and anisotropic on the other side (inside the cavity, marked with a subscript $+$), and using Eq. (D3), we got the following expressions for the magnetic fields on each side of the layer:

$$\boldsymbol{H}_{0^-} = \mathbf{S}_{12,-}^{-1} \partial_z \boldsymbol{E}_{0^-}, \tag{F4a}$$

$$\boldsymbol{H}_{0^+} = \mathbf{S}_{12,+}^{-1} \partial_z \boldsymbol{E}_{0^+} - \mathbf{S}_{12,+}^{-1}\mathbf{S}_{11,+}\boldsymbol{E}_{0^+}. \tag{F4b}$$

In the next step we eliminate the magnetic field using Eq. (F3) leading in the limit of $|\zeta|/k_0 \gg 1 \gg \kappa$ to

$$\begin{bmatrix} \boldsymbol{E}_{0^+} \\ \partial_z \boldsymbol{E}_{0^+} \end{bmatrix} = \begin{bmatrix} \boldsymbol{\sigma}_0 & \mathbf{0} \\ 2\zeta\boldsymbol{\sigma}_0 & \boldsymbol{\sigma}_0 \end{bmatrix} \begin{bmatrix} \boldsymbol{E}_{0^-} \\ \partial_z \boldsymbol{E}_{0^-} \end{bmatrix} = \hat{M} \begin{bmatrix} \boldsymbol{E}_{0^-} \\ \partial_z \boldsymbol{E}_{0^-} \end{bmatrix}. \quad (F5)$$

In this limit we omit the TE-TM splitting on the δ mirrors. To take into account the TE-TM splitting at the mirrors we cannot assume that $\mathbf{S}_{12,+} \approx \mathbf{S}_{12,-}$. As a result, the electric field is continuous across the thin film, but its derivative has a discontinuity. An analogous situation occurs in the quantum mechanical problem of scattering by the Dirac δ potential. Our optical cavity model, in which Bragg mirrors are replaced by thin layers of material with high refractive index, somewhat resembles a quantum particle enclosed in a quantum well with δ-like barriers.

2. Reflection and transmission coefficients

The relation between electric and magnetic fields on both sides of an anisotropic medium in a cavity is defined by Eq. (D3). Using the standard procedure in this case and changing the magnetic field to the derivative of the electric field yields the following:

$$\begin{bmatrix} \boldsymbol{E}_{L^-} \\ \partial_z \boldsymbol{E}_{L^-} \end{bmatrix} = \hat{T} \begin{bmatrix} \boldsymbol{E}_{0^+} \\ \partial_z \boldsymbol{E}_{0^+} \end{bmatrix}, \quad (F6a)$$

$$\hat{T} = \begin{bmatrix} \boldsymbol{\sigma}_0 & \mathbf{0} \\ \mathbf{S}_{11} & \mathbf{S}_{12} \end{bmatrix} \exp\left(\begin{bmatrix} \mathbf{S}_{11} & \mathbf{S}_{12} \\ \mathbf{S}_{21} & \mathbf{S}_{22} \end{bmatrix} L \right)$$
$$\times \begin{bmatrix} \boldsymbol{\sigma}_0 & \mathbf{0} \\ -\mathbf{S}_{12}^{-1}\mathbf{S}_{11} & \mathbf{S}_{12}^{-1} \end{bmatrix}, \quad (F6b)$$

where L is the width of the anisotropic medium (distance between two δ mirrors), and $\boldsymbol{E}_{L^-}$, $\partial_z\boldsymbol{E}_{L^-}$, $\boldsymbol{E}_{0^+}$, and $\partial_z\boldsymbol{E}_{0^+}$ denote the electric field and its derivative on the left and right sides of the anisotropic medium, respectively. The total transfer matrix for the cavity with δ mirrors is

$$\begin{bmatrix} \boldsymbol{E}_{L^+} \\ \partial_z \boldsymbol{E}_{L^+} \end{bmatrix} = \hat{M}\hat{T}\hat{M} \begin{bmatrix} \boldsymbol{E}_{0^-} \\ \partial_z \boldsymbol{E}_{0^-} \end{bmatrix}, \quad (F7)$$

where $\boldsymbol{E}_{L^+}$, $\partial_z\boldsymbol{E}_{L^+}$, $\boldsymbol{E}_{0^-}$, and $\partial_z\boldsymbol{E}_{0^-}$ denote the electric field and its derivative on the right side and the left side of the right and left δ mirrors, respectively. To determine the expression for reflection and transmission coefficients we considered standard scattering geometry (with incident wave from the left) in which the two-dimensional vector of the electric field in the x-y plane for incident $\boldsymbol{E}_{in}$, reflected $\boldsymbol{E}_{re}$, and transmitted $\boldsymbol{E}_{tr}$ waves were given by

$$\boldsymbol{E}_{in}(x, y, z) = \boldsymbol{E}_{in,0} e^{i(k_0 \boldsymbol{\kappa} \cdot \boldsymbol{r} + k_0 \kappa_z z - \omega t)}, \quad (F8a)$$

$$\boldsymbol{E}_{re}(x, y, z) = \boldsymbol{E}_{re,0} e^{i(k_0 \boldsymbol{\kappa} \cdot \boldsymbol{r} - k_0 \kappa_z z - \omega t)}, \quad (F8b)$$

$$\boldsymbol{E}_{tr}(x, y, z) = \boldsymbol{E}_{tr,0} e^{i(k_0 \boldsymbol{\kappa} \cdot \boldsymbol{r} + k_0 \kappa_z z - \omega t)}. \quad (F8c)$$

Here $\boldsymbol{E}_{in,0}$, $\boldsymbol{E}_{re,0}$, and $\boldsymbol{E}_{tr,0}$ denote the two-dimensional vectors of the amplitude of the electric field in the x-y plane for incident, reflected, and transmitted waves, respectively, and $\kappa_z = \sqrt{n_a^2 - \kappa_x^2 - \kappa_y^2}$, where n_a is a refractive index for an

isotropic medium outside the cavity. Using Eqs. (F8) and (F7) leads to

$$\begin{bmatrix} \boldsymbol{E}_{tr,0} \\ \mathbf{0} \end{bmatrix} = \hat{F} \begin{bmatrix} \boldsymbol{E}_{in,0} \\ \boldsymbol{E}_{re,0} \end{bmatrix} = \begin{bmatrix} \mathbf{F}_{11} & \mathbf{F}_{12} \\ \mathbf{F}_{21} & \mathbf{F}_{22} \end{bmatrix} \begin{bmatrix} \boldsymbol{E}_{in,0} \\ \boldsymbol{E}_{re,0} \end{bmatrix}, \quad (F9a)$$

$$\hat{F} = \hat{L}_f^{-1}\hat{M}\hat{T}\hat{M}\hat{L}_i, \quad (F9b)$$

$$\hat{L}_f^{-1} = \begin{bmatrix} \boldsymbol{\sigma}_0 & \mathbf{0} \\ -ik_0\kappa_z\boldsymbol{\sigma}_0 & \boldsymbol{\sigma}_0 \end{bmatrix} e^{-ik_0\kappa_z L}, \quad (F9c)$$

$$\hat{L}_i = \begin{bmatrix} \boldsymbol{\sigma}_0 & \boldsymbol{\sigma}_0 \\ ik_0\kappa_z\boldsymbol{\sigma}_0 & -ik_0\kappa_z\boldsymbol{\sigma}_0 \end{bmatrix}, \quad (F9d)$$

and $\mathbf{F}_{ij}$ are 2×2 submatrices of the matrix $\hat{F}$. The matrices $\hat{L}_f^{-1}$ and $\hat{L}_i$ are analogous to the matrices introduced in Ref. [39] and describe the transformation of $\boldsymbol{E}_{L^+}$ and $\partial_z\boldsymbol{E}_{L^+}$ to the amplitude of the transmitted wave and the amplitudes of the incident and reflected waves to $\boldsymbol{E}_{0^-}$ and $\partial_z\boldsymbol{E}_{0^-}$, respectively. Solving Eq. (F9a) yields the following expressions for the amplitude of reflected and transmitted waves:

$$\boldsymbol{E}_{re,0} = -\mathbf{F}_{22}^{-1}\mathbf{F}_{21}\boldsymbol{E}_{in,0}, \quad (F10a)$$

$$\boldsymbol{E}_{tr,0} = \left(\mathbf{F}_{11} - \mathbf{F}_{12}\mathbf{F}_{22}^{-1}\mathbf{F}_{21}\right)\boldsymbol{E}_{in,0}. \quad (F10b)$$
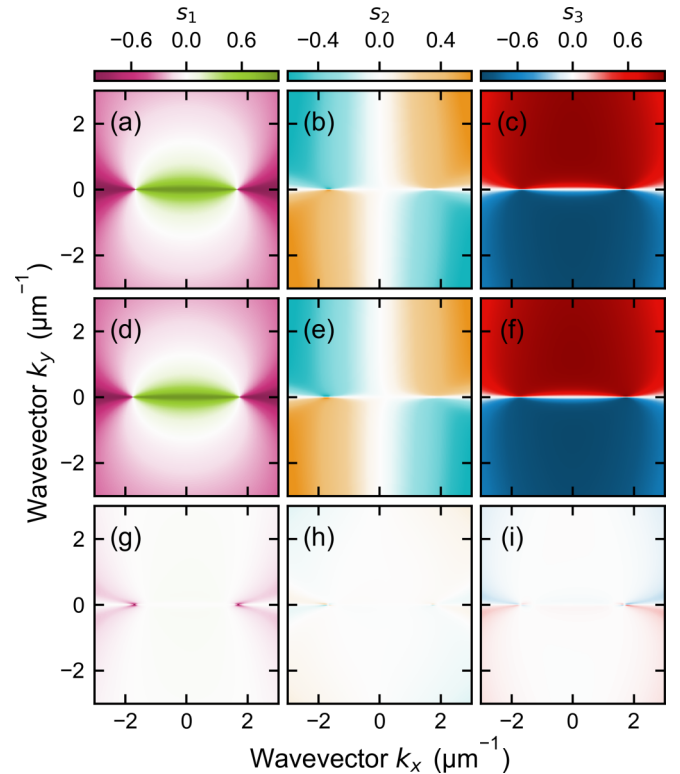

FIG. 8. Stokes polarization parameters [(a), (d), (g)] s_1, [(b), (e), (h)] s_2, and [(c), (f), (i)] s_3 for the upper energy branch for different values of $\boldsymbol{k}$, respectively, obtained by using [(a)–(c)] the transfer matrix method according to the procedure described in Appendix F, and [(d)–(f)] diagonalization of the multimode Hamiltonian (32), respectively. In the bottom row we present the difference between results presented in the top row and in Figs. 4(a)–4(c).
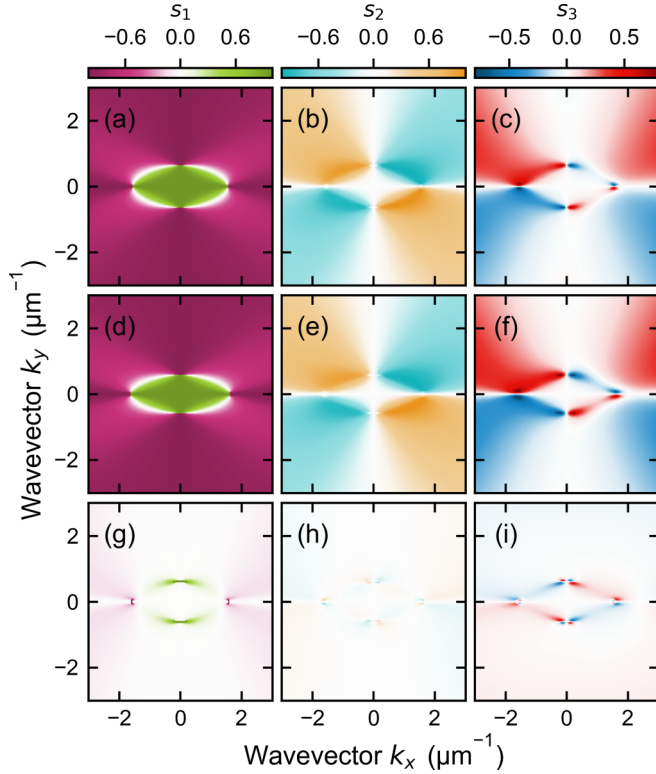
FIG. 9. Stokes polarization parameters [(a), (d), (g)] s_1, [(b), (e), (h)] s_2, and [(c), (f), (i)] s_3 for the upper energy branch for different values of $\boldsymbol{k}$, respectively, obtained by using [(a)–(c)] the transfer matrix method according to the procedure described in Appendix F, and [(d)–(f)] diagonalization of multimode Hamiltonian (32), respectively. In the bottom row we present the difference between results presented in the top row and in Figs. 5(a)–5(c).
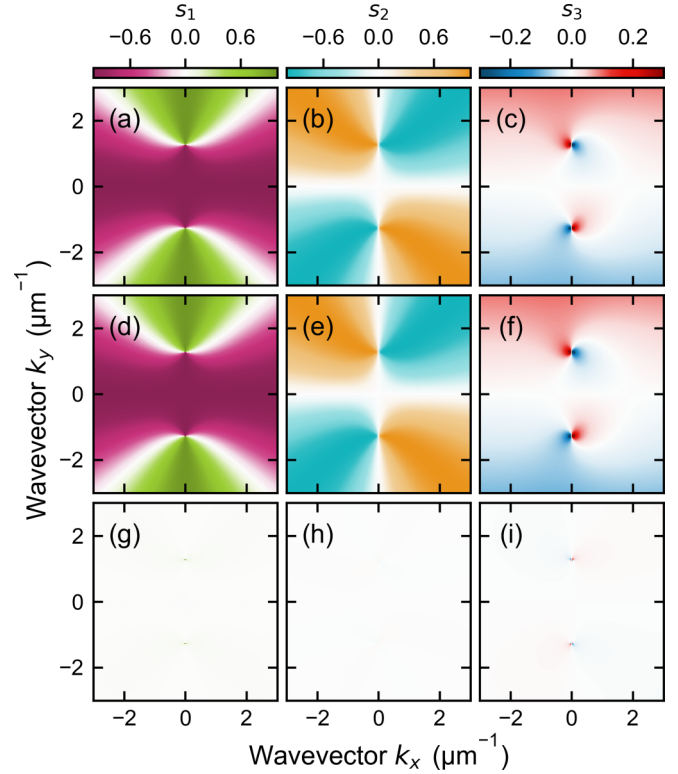
FIG. 10. Stokes polarization parameters [(a), (d), (g)] s_1, [(b), (e), (h)] s_2, and [(c), (f), (i)] s_3 for the upper energy branch for different values of $\boldsymbol{k}$, respectively, obtained by using [(a)–(c)] the transfer matrix method according to the procedure described in Appendix F, and [(d)–(f)] diagonalization of multimode Hamiltonian (32), respectively. In the bottom row we present the difference between results presented in the top row and in Figs. 6(a)–6(c).

3. Outgoing wave boundary condition

The amplitude of the incident wave in the case of outgoing wave boundary conditions is equal to zero, so according to Eq. (F9a) we get the following equations:

$$
\begin{bmatrix} -\boldsymbol{\sigma}_0 & \mathbf{F}_{12} \\ \mathbf{0} & \mathbf{F}_{22} \end{bmatrix} \begin{bmatrix} \boldsymbol{E}_{tr,0} \\ \boldsymbol{E}_{re,0} \end{bmatrix} = \begin{bmatrix} \mathbf{0} \\ \mathbf{0} \end{bmatrix}. \tag{F11}
$$

Similarly to Refs. [50,51], nontrivial solutions occur when the determinant of the matrix in Eq. (F11) is equal to zero, so

$$
\det(\mathbf{F}_{22}) = 0. \tag{F12}
$$

In this case, we get complex solutions for which the real and imaginary parts correspond to the resonant energy and the width of the mode, respectively. The complex roots were found using the standard Newton algorithm for complex numbers with initial value determined as eigenvalues of the 2×2 Hamiltonian matrix for each regime.

APPENDIX G: COMPARISON OF THE EFFECTIVE TWO-MODE APPROXIMATION WITH MULTIMODE AND BERREMAN-SCHUBERT METHODS

In this Appendix, we compare the Stokes parameters calculated using different models in three discussed regimes $X(m')$, $Y(m)$ of almost degenerate modes: (i) $X(m+1)$ and $Y(m)$ (Fig. 8), (ii) $X(m+2)$ and $Y(m)$ (Fig. 9), and (iii) $X(m)$ and $Y(m)$ (Fig. 10). We verified our two-mode approximation using more accurate methods, one of which included the standard Berreman approach for a cavity with δ mirrors for outgoing wave boundary conditions presented in Appendix F [Figs. 8(a)–8(c), 9(a)–9(c), and 10(a)–10(c)], and the band multimode Hamiltonian (32) [Figs. 8(d)–8(f), 9(d)–9(f), and 10(d)–10(f)]. For each regime we present Stokes polarization parameters for the upper energy branch for different $\boldsymbol{k}$, and additionally the polarization differences between dispersion relations according to the procedure in Appendix F and by diagonalization of two-mode Hamiltonians (45), (47), and (49) for Figs. 8(g)–8(i), 9(g)–9(i), and 10(g)–10(i), respectively. The main differences between the models are caused by the omission of higher-order terms in the two-mode approximation in which we take into account only linear terms [see Eqs. (36) and (38)]. Nevertheless, these results prove that

the two-mode Hamiltonians supplemented with the formulas presented in Appendix E accurately reproduce all polarization patterns. Therefore, we have successfully simplified the description of the interactions between modes.

[1] I. Bialynicki-Birula, Photon wave function, in *Progress in Optics* (Elsevier, Amsterdam, 1996), pp. 245–294.

[2] M. G. Silveirinha, Chern invariants for continuous media, Phys. Rev. B **92**, 125153 (2015).

[3] K. Y. Bliokh, F. J. Rodríguez-Fortuño, F. Nori, and A. V. Zayats, Spin-orbit interactions of light, Nat. Photonics **9**, 796 (2015).

[4] V. S. Liberman and B. Y. Zel'dovich, Spin-orbit interaction of a photon in an inhomogeneous medium, Phys. Rev. A **46**, 5199 (1992).

[5] K. Y. Bliokh, Geometrodynamics of polarized light: Berry phase and spin Hall effect in a gradient-index medium, J. Opt. A: Pure Appl. Opt. **11**, 094009 (2009).

[6] F. Cardano and L. Marrucci, Spin-orbit photonics, Nat. Photonics **9**, 776 (2015).

[7] E. A. Muljarov, W. Langbein, and R. Zimmermann, Brillouin-Wigner perturbation theory in open electromagnetic systems, Europhys. Lett. **92**, 50010 (2010).

[8] E. A. Muljarov and W. Langbein, Exact mode volume and Purcell factor of open optical systems, Phys. Rev. B **94**, 235438 (2016).

[9] P. S. Y. Poon and C. K. Law, Polarization and frequency disentanglement of photons via stochastic polarization mode dispersion, Phys. Rev. A **77**, 032330 (2008).

[10] T. Ozawa, H. M. Price, A. Amo, N. Goldman, M. Hafezi, L. Lu, M. C. Rechtsman, D. Schuster, J. Simon, O. Zilberberg, and I. Carusotto, Topological photonics, Rev. Mod. Phys. **91**, 015006 (2019).

[11] L. Lu, J. D. Joannopoulos, and M. Soljačić, Topological photonics, Nat. Photonics **8**, 821 (2014).

[12] D. D. Solnyshkov, G. Malpuech, P. St-Jean, S. Ravets, J. Bloch, and A. Amo, Microcavity polaritons for topological photonics [invited], Opt. Mater. Express **11**, 1119 (2021).

[13] A. Kavokin, G. Malpuech, and M. Glazov, Optical spin Hall effect, Phys. Rev. Lett. **95**, 136601 (2005).

[14] C. Leyder, M. Romanelli, J. P. Karr, E. Giacobino, T. C. H. Liew, M. M. Glazov, A. V. Kavokin, G. Malpuech, and A. Bramati, Observation of the optical spin Hall effect, Nat. Phys. **3**, 628 (2007).

[15] K. Lekenta, M. Król, R. Mirek, K. Lempicka, D. Stephan, R. Mazur, P. Morawiak, P. Kula, W. Piecek, P. G. Lagoudakis, B. Pietka, and J. Szczytko, Tunable optical spin Hall effect in a liquid crystal microcavity, Light Sci. Appl. **7**, 74 (2018).

[16] K. Rechcińska, M. Król, R. Mazur, P. Morawiak, R. Mirek, K. Łempicka, W. Bardyszewski, M. Matuszewski, P. Kula, W. Piecek, P. G. Lagoudakis, B. Piętka, and J. Szczytko, Engineering spin-orbit synthetic Hamiltonians in liquid-crystal optical cavities, Science **366**, 727 (2019).

[17] T. Long, X. Ma, J. Ren, F. Li, Q. Liao, S. Schumacher, G. Malpuech, D. Solnyshkov, and H. Fu, Helical polariton lasing from topological valleys in an organic crystalline microcavity, Adv. Sci. **9**, 2203588 (2022).

[18] Y. Li, X. Ma, X. Zhai, M. Gao, H. Dai, S. Schumacher, and T. Gao, Manipulating polariton condensates by Rashba-Dresselhaus coupling at room temperature, Nat. Commun. **13**, 3785 (2022).

[19] L. Polimeno, G. Lerario, M. D. Giorgi, L. D. Marco, L. Dominici, F. Todisco, A. Coriolano, V. Ardizzone, M. Pugliese, C. T. Prontera, V. Maiorano, A. Moliterni, C. Giannini, V. Olieric, G. Gigli, D. Ballarini, Q. Xiong, A. Fieramosca, D. D. Solnyshkov, G. Malpuech *et al.*, Tuning of the Berry curvature in 2D perovskite polaritons, Nat. Nanotechnol. **16**, 1349 (2021).

[20] Q. Liao, C. Leblanc, J. Ren, F. Li, Y. Li, D. Solnyshkov, G. Malpuech, J. Yao, and H. Fu, Experimental measurement of the divergent quantum metric of an exceptional point, Phys. Rev. Lett. **127**, 107402 (2021).

[21] J. Ren, Q. Liao, F. Li, Y. Li, O. Bleu, G. Malpuech, J. Yao, H. Fu, and D. Solnyshkov, Nontrivial band geometry in an optically active system, Nat. Commun. **12**, 689 (2021).

[22] M. S. Spencer, Y. Fu, A. P. Schlaus, D. Hwang, Y. Dai, M. D. Smith, D. R. Gamelin, and X.-Y. Zhu, Spin-orbit coupled exciton-polariton condensates in lead halide perovskites, Sci. Adv. **7**, eabj7667 (2021).

[23] M. Muszyński, M. Król, K. Rechcińska, P. Oliwa, M. Kedziora, K. Łempicka-Mirek, R. Mazur, P. Morawiak, W. Piecek, P. Kula, P. G. Lagoudakis, B. Piętka, and J. Szczytko, Realizing persistent-spin-helix lasing in the regime of Rashba-Dresselhaus spin-orbit coupling in a dye-filled liquid-crystal optical microcavity, Phys. Rev. Appl. **17**, 014041 (2022).

[24] J. Ren, Q. Liao, X. Ma, S. Schumacher, J. Yao, and H. Fu, Realization of exciton-mediated optical spin-orbit interaction in organic microcrystalline resonators, Laser Photonics Rev. **16**, 2100252 (2021).

[25] C. Rupprecht, E. Sedov, M. Klaas, H. Knopf, M. Blei, N. Lundt, S. Tongay, T. Taniguchi, K. Watanabe, U. Schulz, A. Kavokin, F. Eilenberger, S. Höfling, and C. Schneider, Manipulation of room-temperature valley-coherent exciton-polaritons in atomically thin crystals by real and artificial magnetic fields, 2D Mater. **7**, 035025 (2020).

[26] K. Łempicka-Mirek, M. Król, H. Sigurdsson, A. Wincukiewicz, P. Morawiak, R. Mazur, M. Muszyński, W. Piecek, P. Kula, T. Stefaniuk, M. Kamińska, L. D. Marco, P. G. Lagoudakis, D. Ballarini, D. Sanvitto, J. Szczytko, and B. Piętka, Electrically tunable Berry curvature and strong light-matter coupling in liquid crystal microcavities with 2D perovskite, Sci. Adv. **8**, 40 (2022).

[27] L. Polimeno, A. Fieramosca, G. Lerario, L. D. Marco, M. D. Giorgi, D. Ballarini, L. Dominici, V. Ardizzone, M. Pugliese, C. T. Prontera, V. Maiorano, G. Gigli, C. Leblanc, G. Malpuech, D. D. Solnyshkov, and D. Sanvitto, Experimental investigation of a non-Abelian gauge field in 2D perovskite photonic platform, Optica **8**, 1442 (2021).

[28] D. Biegańska, M. Pieczarka, E. Estrecho, M. Steger, D. W. Snoke, K. West, L. N. Pfeiffer, M. Syperek, A. G. Truscott, and E. A. Ostrovskaya, Collective excitations of exciton-polariton

condensates in a synthetic gauge field, Phys. Rev. Lett. **127**, 185301 (2021).

[29] A. Li, H. Wei, M. Cotrufo, W. Chen, S. Mann, X. Ni, B. Xu, J. Chen, J. Wang, S. Fan, C.-W. Qiu, A. Alù, and L. Chen, Exceptional points and non-Hermitian photonics at the nanoscale, Nat. Nanotechnol. **18**, 706 (2023).

[30] P. Kokhanchik, H. Sigurdsson, B. Piętka, J. Szczytko, and P. G. Lagoudakis, Photonic Berry curvature in double liquid crystal microcavities with broken inversion symmetry, Phys. Rev. B **103**, L081406 (2021).

[31] W. Zhu, H. Zheng, Y. Zhong, J. Yu, and Z. Chen, Wave-vector-varying Pancharatnam-Berry phase photonic spin Hall effect, Phys. Rev. Lett. **126**, 083901 (2021).

[32] A. Gianfrate, O. Bleu, L. Dominici, V. Ardizzone, M. D. Giorgi, D. Ballarini, G. Lerario, K. W. West, L. N. Pfeiffer, D. D. Solnyshkov, D. Sanvitto, and G. Malpuech, Measurement of the quantum geometric tensor and of the anomalous Hall drift, Nature (London) **578**, 381 (2020).

[33] M. Król, H. Sigurdsson, K. Rechcińska, P. Oliwa, K. Tyszka, W. Bardyszewski, A. Opala, M. Matuszewski, P. Morawiak, R. Mazur, W. Piecek, P. Kula, P. G. Lagoudakis, B. Piętka, and J. Szczytko, Observation of second-order meron polarization textures in optical microcavities, Optica **8**, 255 (2021).

[34] D. D. Solnyshkov, C. Leblanc, L. Bessonart, A. Nalitov, J. Ren, Q. Liao, F. Li, and G. Malpuech, Quantum metric and wave packets at exceptional points in non-Hermitian systems, Phys. Rev. B **103**, 125302 (2021).

[35] M. Król, I. Septembre, P. Oliwa, M. Kędziora, K. Łempicka-Mirek, M. Muszyński, R. Mazur, P. Morawiak, W. Piecek, P. Kula, W. Bardyszewski, P. G. Lagoudakis, D. D. Solnyshkov, G. Malpuech, B. Piętka, and J. Szczytko, Annihilation of exceptional points from different Dirac valleys in a 2D photonic system, Nat. Commun. **13**, 5340 (2022).

[36] R. Su, E. Estrecho, D. Biegańska, Y. Huang, M. Wurdack, M. Pieczarka, A. G. Truscott, T. C. H. Liew, E. A. Ostrovskaya, and Q. Xiong, Direct measurement of a non-Hermitian topological invariant in a hybrid light-matter system, Sci. Adv. **7**, eabj8905 (2021).

[37] R. M. More and E. Gerjuoy, Properties of resonance wave functions, Phys. Rev. A **7**, 1288 (1973).

[38] D. W. Berreman, Optics in stratified and anisotropic media: 4×4-Matrix formulation, J. Opt. Soc. Am. **62**, 502 (1972).

[39] M. Schubert, Polarization-dependent optical parameters of arbitrarily anisotropic homogeneous layered systems, Phys. Rev. B **53**, 4265 (1996).

[40] G. M. A. Kavokin, *Cavity Polaritons* (Elsevier, Amsterdam, 2003).

[41] G. M. A. Kavokin, *Exciton Polaritons in Microcavities: New Frontiers* (Springer-Verlag, Berlin, 2012).

[42] R. C. Jones, A new calculus for the treatment of optical systems. IV., J. Opt. Soc. Am. **32**, 486 (1942).

[43] M. Król, K. Rechcińska, H. Sigurdsson, P. Oliwa, R. Mazur, P. Morawiak, W. Piecek, P. Kula, P. G. Lagoudakis, M. Matuszewski, W. Bardyszewski, B. Piętka, and J. Szczytko, Realizing optical persistent spin helix and Stern-Gerlach deflection in an anisotropic liquid crystal microcavity, Phys. Rev. Lett. **127**, 190401 (2021).

[44] T. Berggren and P. Lind, Resonant state expansion of the resolvent, Phys. Rev. C **47**, 768 (1993).

[45] G. García-Calderón and R. Peierls, Resonant states and their uses, Nucl. Phys. A **265**, 443 (1976).

[46] P. M. Morse and H. Feshbach, *Methods of Theoretical Physics* (McGraw-Hill, New York, 1953).

[47] V. V. Konotop, J. Yang, and D. A. Zezyulin, Nonlinear waves in $\mathcal{PT}$-symmetric systems, Rev. Mod. Phys. **88**, 035002 (2016).

[48] R. G. Newton, Analytic properties of radial wave functions, J. Math. Phys. **1**, 319 (1960).

[49] L. L. Foldy and S. A. Wouthuysen, On the Dirac theory of spin 1/2 particles and its non-relativistic limit, Phys. Rev. **78**, 29 (1950).

[50] S. Richter, T. Michalsky, C. Sturm, B. Rosenow, M. Grundmann, and R. Schmidt-Grund, Exceptional points in anisotropic planar microcavities, Phys. Rev. A **95**, 023836 (2017).

[51] S. Richter, H.-G. Zirnstein, J. Zúñiga-Pérez, E. Krüger, C. Deparis, L. Trefflich, C. Sturm, B. Rosenow, M. Grundmann, and R. Schmidt-Grund, Voigt exceptional points in an anisotropic ZnO-based planar microcavity: Square-root topology, polarization vortices, and circularity, Phys. Rev. Lett. **123**, 227401 (2019).

[52] J. Yang, C. Qian, X. Xie, K. Peng, S. Wu, F. Song, S. Sun, J. Dang, Y. Yu, S. Shi, J. He, M. J. Steer, I. G. Thayne, B.-B. Li, F. Bo, Y.-F. Xiao, Z. Zuo, K. Jin, C. Gu, and X. Xu, Diabolical points in coupled active cavities with quantum emitters, Light Sci. Appl. **9**, 6 (2020).